



Cite this: DOI: 10.1039/c9dt00921c

Luminescent anticancer ruthenium(II)-*p*-cymene complexes of extended imidazophenanthroline ligands: synthesis, structure, reactivity, biomolecular interactions and live cell imaging†

Bidisha Sarkar, ^{‡a} Ashaparna Mondal, ^{‡a} Yukti Madaan, ^a Nilmadhab Roy, ^a Anbalagan Moorthy, ^b Yung-Chih Kuo ^c and Priyanka Paira ^{*a}

Of late, cancer has become a terrible disease affecting people throughout the world. Keeping this in mind, we tried to design drugs that are more lipophilic, target-specific, water-soluble, cytoselective and fluorescent. In this regard, we reported novel ruthenium(II)-*p*-cymene imidazophenanthroline scaffolds as effective DNA targeting agents. The planarity of imidazophenanthroline ligands caused the Ru(II) complex to be a good intercalator. An extended π -electronic conjugation was introduced in the imidazophenanthroline moieties through the Suzuki and Sonogashira coupling reactions. Here, we synthesized nine Ru(II) complexes (**16a–b**, **17a–d**, and **19a–c**). Among these, $[(\eta^6\text{-}p\text{-cymene})\text{RuCl}(\text{K}^2\text{-}N,N\text{-}2\text{-}(4'\text{-methyl-[1,1'-B]phenyl)-4-yl)-1H-imidazo[4,5-f][1,10]phenanthroline})]\cdot\text{PF}_6$ (**16b**) exhibited the best potency and selectivity with excellent cellular uptake; $[(\eta^6\text{-}p\text{-cymene})\text{RuCl}(\text{K}^2\text{-}N,N\text{-}2\text{-}(4\text{-}(phenylethynyl)phenyl)-1H-imidazo[4,5-f][1,10]phenanthroline})]\cdot\text{PF}_6$ (**17a**) acted as a cytoselective probe for live cell imaging.

Received 1st March 2019,
Accepted 8th July 2019

DOI: 10.1039/c9dt00921c

rsc.li/dalton

Introduction

Cancer is the second most life-threatening disease around the world after heart disease, and it is mainly caused by the mutation in genes, which leads to abnormal and unrestricted cell growth.¹ Chemotherapy is the most prevalent traditional cancer therapy, but it is inefficient in terms of tumor specificity, hence rendering normal cells at risk. Targeted therapy can only disrupt the process of carcinogenesis. Metal complexes have played an important role in medicine for around 5000 years because of their physico-chemical properties, variable oxidation states, hydrophobicity and lipophilicity, high aqueous solubility and positively charged nature.^{2–9} Cisplatin, the first FDA (Food Drug Administration)-approved anticancer platinum(II) drug, is used for the treatment of a large variety of cancers such as ovarian, lung, oesophageal, neck, cervical and

brain cancers.^{10–12} Various other second-generation platinum drugs such as carboplatin and oxaloplatin are also used. However, the use of these platinum drugs towards cancer treatment is being reduced because of their poor aqueous solubility, toxicity to normal cells and drug-resistance problems.^{13–24} Ruthenium complexes have displayed promising results as the next possible anticancer therapeutics due to their high rate of ligand exchange, a wide range of accessible oxidation states, and exceptional aqueous solubility and stability in a biological environment.²⁵ In general, ruthenium shows anticancer activity in its +2 oxidation state when reduced from the +3 state *in vivo* as ruthenium(III) complexes are relatively unreactive due to higher electrostatic pull from the nucleus. The reduction from ruthenium(III) to ruthenium(II) is most likely to occur in a cancer cellular environment as it is acidic, has a lower oxygen content and has a higher glutathione concentration.^{26–28} Hence ruthenium(III) complexes can selectively treat cancer cells without disturbing the growth of normal cells as they are inert to normal cells. NAMI-A and KP1019 are two ruthenium(III) drugs that have reached clinical trials so far. There are studies that support the binding of NAMI-A with DNA and histidine of serum albumins (HSA) in biological systems.^{29–31} NAMI-A showed low efficacy against the progress of the disease in phase I of the clinical trial, which restricted its use for further clinical trials.³² Consequently, Keppler *et al.* developed KP1019, which has

^aDepartment of Chemistry, School of Advanced Sciences, VIT, Vellore-632014, Tamil Nadu, India. E-mail: priyanka.paira@vit.ac.in; Fax: +91-416-2243092; Tel: +91-416-2243091

^bDepartment of Biotechnology, School of Bioscience & Technology, Vellore Institute of Technology, Vellore 632014, Tamil Nadu, India

^cDepartment of Chemical Engineering, National Chung Cheng University, 168, University Rd., Chia-Yi, Min-Hsiung, Taiwan 62102

†Electronic supplementary information (ESI) available. See DOI: 10.1039/c9dt00921c

‡Equal contribution.

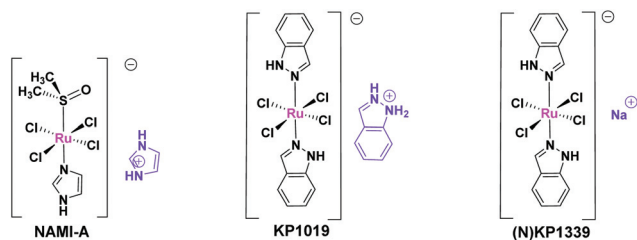


Fig. 1 Structures of NAMI-A, KP1019 and KP1339.

since moved into the clinical investigation stage.^{33,34} Also, as a result of its solubility problem, its sodium salt KP1339 is undergoing clinical investigations³⁵ (Fig. 1).

The hydrophobic character of the arene ligand attached to ruthenium facilitates the passive diffusion of the complex through the cell membrane and enhances its cellular accumulation.³⁶ To support this phenomenon, Sadler *et al.* reported a family of piano-stool ruthenium(II)-arene pyridyl complexes of the type $[(\eta^6\text{-arene})\text{Ru}(N,N')(\text{L})][\text{PF}_6]_2$ for photoactivation and ruthenium(II) arene complexes containing *N,N*-, *N,O*- and *O,O*-chelating ligands for anticancer activity.^{37–39}

DNA and proteins have distinct structures and functions and they both play acute roles in regulating cellular functions.^{40,41} Hence, close investigation of the interactions of ruthenium complexes with DNA and proteins is mandatory to understand the anticancer mechanism and to design an efficient target-specific drug. A variety of ruthenium complexes have been reported to bind with DNA either in covalent mode or in non-covalent mode.^{42–46} For example, the ruthenium complex $[\text{Ru}(\eta^6\text{-biphenyl})(\text{en})\text{Cl}]^+[\text{PF}_6]^-$ specifically binds to guanine in aqueous environment, unlike adenine, thymine and cytosine.^{47–49} Thus this kind of covalent binding deforms the DNA backbone, which spoils DNA transcription and replication. The non-covalent binding is reversible in nature and it can be further divided into various types, like groove binding, electrostatic binding and intercalation. Ruthenium(II) complexes can undergo intercalation when they have planar aromatic ligands and the complex gets inserted in between adjacent base pairs of DNA.⁵⁰ Liu *et al.* reported two Ru(II) polypyridyl complexes, namely $[\text{Ru}(2,2'\text{-bpy})_2(\text{MCMIP})]^{2+}$ (1) and $[\text{Ru}(\text{phen})_2(\text{MCMIP})]^{2+}$ (2), for cancer therapy. These two complexes bind to DNA through intercalation in between base pairs.⁵¹ Tan *et al.* developed two novel Ru(II) polypyridyl complexes, namely $[\text{Ru}(\text{bpy})_2(\text{BPIP})]^{2+}$ (3) and $[\text{Ru}(\text{phen})_2(\text{BPIP})]^{2+}$ (4), which also bind to CT-DNA *via* intercalation.⁵² Kumar *et al.* reported three Ru(II) complexes, namely $[\text{Ru}(\text{bipy})_2\text{PRIP}]^{2+}$ (5), $[\text{Ru}(\text{dmb})_2\text{PRIP}]^{2+}$ (6) and $[\text{Ru}(\text{phen})_2\text{PRIP}]^{2+}$ (7), which were found to intercalate in between DNA base pairs through the aromatic ligand PRIP⁵³ (Fig. 2). However, the development of novel ruthenium(II)-arene complexes with extended π -conjugation is still a challenge for target-oriented cancer therapy and cellular imaging.

In continuation of our ongoing work on anticancer organo-rutheniums,⁵⁴ in the present study, we designed complexes

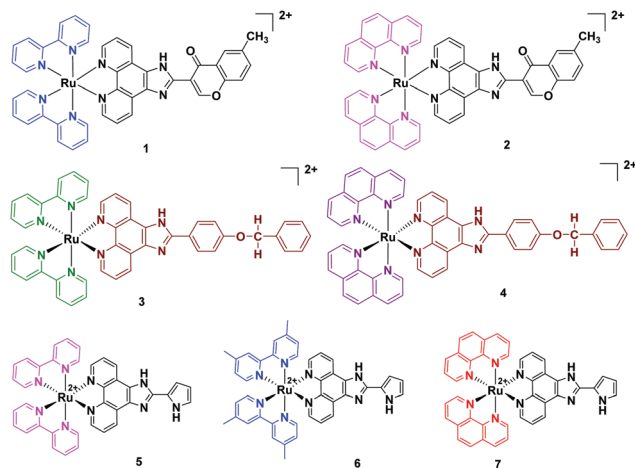


Fig. 2 Structures of some Ru(II) polypyridyl-type complexes.

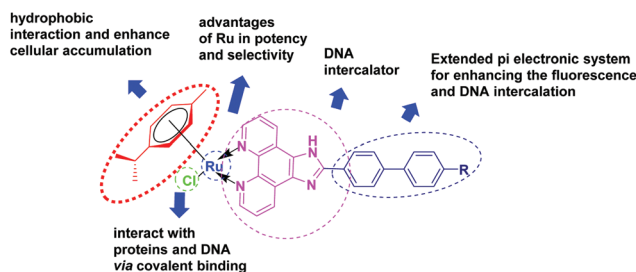


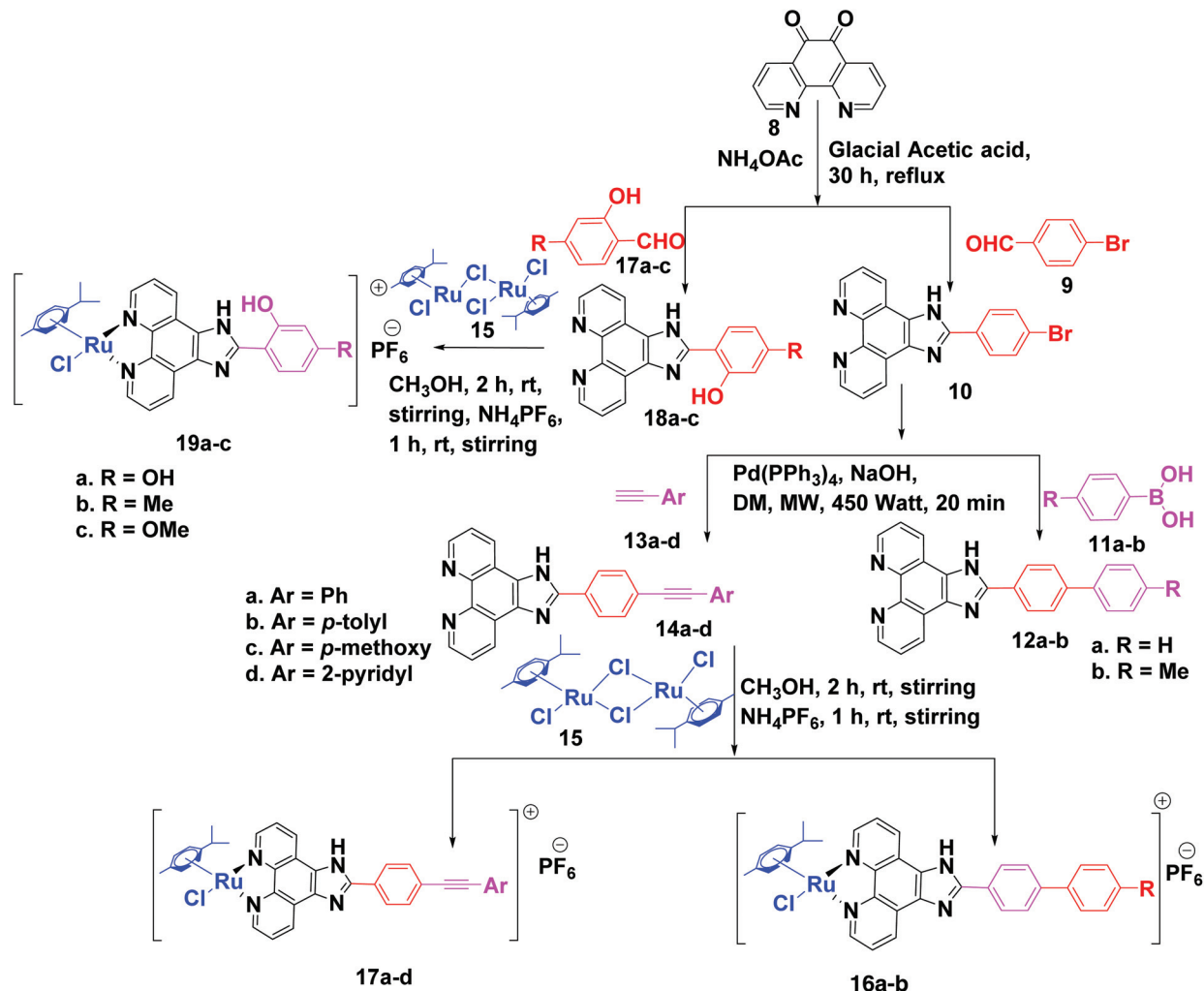
Fig. 3 Design of Ru(II)-imidazophenanthroline complexes.

having some crucial units, like: (i) a labile chlorine ligand for facilitating biomolecular interactions;⁵⁵ (ii) a η^6 -*p*-cymene moiety for stabilizing the oxidation state of ruthenium and to increase the potency of drug transportation into the cell membrane;^{56,57} (iii) *d*⁶ transition metal ruthenium for potency and selectivity; and (iv) extended π -conjugated ligands for cellular imaging and DNA intercalation. Herein for reporting, we selected a variety of imidazophenanthroline analogues as ligands along with ruthenium(II)-*p*-cymene precursors for the synthesis of bioactive metal complexes (Fig. 3).

Results and discussion

Synthesis and characterization

At the outset, 2-(4-bromophenyl)-1*H*-imidazo[4,5-*f*][1,10]phenanthroline (10) was prepared in a conventional way by the condensation of 1,10-phenanthroline-5,6-dione (8) and 4-bromobenzaldehyde (9), taken in a 1 : 1 proportion in the presence of NH_4OAc and glacial acetic acid (Scheme 1). The product (10) was fully characterized by ¹H, ¹³C NMR, IR and mass spectroscopy. All 10 aromatic protons of compound 10 appeared in the region of δ 7.78–9.02 ppm in the ¹H NMR spectra. The protons adjacent to the nitrogen atom of the phenanthroline ring appeared as a doublet in the most downfield region of δ



Scheme 1 Synthetic route of Ru(II)-arene imidazophenanthroline complexes.

9.01–9.02 ppm. In the ¹³C NMR, peaks of six quaternary carbons and five tertiary carbons were also observed. The C–Br stretching frequency was obtained at 619 cm⁻¹ in the IR spectra, which indicated the presence of C–Br bonds in compound **10**. The LCMS peak at *m/z*: 375.2 [M + H]⁺ confirmed the formation of compound **10**.

Suzuki coupling was performed with the above compound (**10**) and benzene boronic acid (**11a**) in the presence of 10 mol% (PPh₃)₄Pd and NaOH in DMF under microwave irradiation (450 W, 150 °C, 15 min). The desired ligand 2-([1,1'-biphenyl]-4-yl)-1*H*-imidazo[4,5-*f*][1,10]phenanthroline (**12a**) was isolated in a high yield. The ligand **12a** was fully characterized by ¹H, ¹³C NMR, IR and mass spectroscopy. All 15 aromatic protons of compound **12a** appeared in the region of δ 7.43–9.02 ppm in the ¹H NMR spectra. The proton adjacent to the nitrogen atom of the phenanthroline ring appeared as a broad singlet in the most downfield region of δ 9.02 ppm. In the ¹³C NMR spectra, 10 quaternary carbons peaks and 8 CH peaks were also observed. There was an absence of the C–Br stretching peak at 619 cm⁻¹ in the IR spectra, which indicated the formation of

the C–C coupled product. The LCMS peak at *m/z*: 373.1 [M + H]⁺ confirmed the formation of ligand **12a**. The scope of this chemistry was also extended in the other Suzuki product (**12b**). A Sonogashira coupling reaction was also performed with compound **10** and phenylacetylene (**13a**) in the presence of 10 mol% (PPh₃)₄Pd, NaOH in DMF solvent under microwave irradiation (450, 150 °C, 15 min). The ligand 2-(4-(phenylethynyl)phenyl)-1*H*-imidazo[4,5-*f*][1,10]phenanthroline (**14a**) was isolated in a high yield. This ligand was fully characterized by ¹H and ¹³C NMR, IR and mass spectroscopy. All 15 aromatic protons of ligand **14a** appeared in the region of δ 7.45–9.01 ppm in the ¹H NMR spectra.

The four protons of the phenanthroline ring appeared as a multiplet in the most downfield region of δ 8.95–9.01 ppm. There was an absence of C–Br stretching at 619 cm⁻¹ in the IR spectrum, which indicated the formation of the C–C coupled product. The scope of this chemistry was also extended to the other Sonogashira analogues (**14b–d**). The ligand 4-(1*H*-imidazo[4,5-*f*][1,10]phenanthrolin-2-yl)benzene-1,3-diol (**18a**) was prepared in a conventional way by the con-

condensation of 1,10-phenanthroline-5,6-dione (**8**) and 2,4-dihydroxybenzaldehyde (**17**), taken in a 1 : 1 proportion in the presence of NH₄OAc and glacial acetic acid. The ligand **18a** was fully characterized by ¹H and ¹³C NMR, IR and mass spectroscopy. All nine aromatic protons of the ligand appeared in the region of 6.46–9.00 ppm in the ¹H NMR spectra. The protons adjacent to the nitrogen atom of the phenanthroline ring appeared as a doublet in the most downfield region of δ 9.02–9.03 ppm and the meta proton of the 2,4-dihydroxybenzaldehyde ring appeared as a singlet at δ 6.46 ppm. The O–H bending at 1404 cm⁻¹ and C–O stretching at 1066 cm⁻¹ confirmed the formation of ligand **18a**. The scope of this chemistry was further extended to **18b–c**.

The Ru(II)-*p*-cymene complex (**16a**) of ligand **12a** was prepared by dissolving the dichloro(*p*-cymene)ruthenium(II) dimer (**15**) in an adequate amount of methanol and adding 2.1 equivalents of ligand **12a** to the reaction mixture followed by magnetic stirring for 2 h. After a change in colour from deep yellow to deep orange, 2.5 equivalents of NH₄PF₆ was added and stirred for another 1 h (Scheme 1). The complex **16a** was fully characterized by ¹H and ¹³C NMR, IR and mass spectroscopy. Due to the formation of a metal complex, the ¹H NMR splitting pattern were changed slightly and all the peaks were shifted towards the downfield region, *i.e.* the ligand peaks in the region of 7.43–9.02 ppm were shifted to 7.43–9.85 ppm in the complex. The characteristic methyl protons of the *p*-cymene ring appeared as a singlet at 2.2 ppm, while the six methyl protons appeared as a doublet at 0.88–0.90 ppm and the CH proton as a multiplet at 2.58–2.62 ppm. The four aromatic protons of the *p*-cymene ring appeared as respective doublets at 6.08–6.10 ppm and 6.32–6.34 ppm. All 19 aromatic protons were observed in the region of δ 6.08–9.85 ppm in the ¹H NMR spectra. The characteristic peaks of phosphorous were observed in the region of δ –153.02 to –135.46 ppm in the ³¹P NMR spectra; whereas specific fluorine peaks of PF₆ were found at δ –71.03 and –69.14 ppm. The P–F stretching at 831 cm⁻¹, sp³ C–H stretching at 2924 cm⁻¹ and sp³ C–H bending at 1460 cm⁻¹ in the IR spectra indicated the formation of a Ru(II) complex. The LCMS peak at m/z : 643.3 [M]⁺ con-

firmed the formation of complex **16a**. The characteristic splitting pattern of the isotopes of ruthenium were also observed in the mass spectra. The same procedure was followed for the synthesis of complexes **16b**, **17a–d** and **19a–c** using various ligands. In complex **17a**, the ligand peaks were observed in the ranges of δ 7.47–9.84 ppm. The methyl group of the *p*-cymene ring appeared as a singlet at 2.2 ppm, the six methyl protons as a doublet at 0.89–0.91 ppm and the CH proton as a multiplet at 2.60–2.63 ppm. The four aromatic protons of the *p*-cymene ring appeared as distinct doublets at 6.10–6.12 ppm and 6.33–6.35 ppm. The LCMS peak at m/z : 667.2 [M]⁺ confirmed the formation of complex **17a**. The complexes **19a–c** were also characterized in a similar fashion.

UV-VIS and fluorescence study

To emphasize the cellular imaging properties of the synthesized Ru(II)-arene complexes (**16a–b**, **17a–d**, **19a–c**), UV and fluorescent studies were conducted in 5% DMSO in PBS at room temperature (Fig. S1†). We observed the λ_{\max} values of these complexes were in the region of 250–450 nm in the UV spectra. Most of the complexes exhibited strong absorption peak at 280–300 nm due to $\pi \rightarrow \pi^*$ transition and a lower energy broad absorption band at 350–450 nm region due to metal-to-ligand charge transfer (MLCT). In order to know the quantum yields (Φ_f) of these complexes, the molecules were excited at λ_{\max} (300–360 nm) and the fluorescence was also recorded (Table 1). Φ_f was calculated by using eqn (ii). Here, we used quinine sulphate as a standard for calculating the emission of the quantum yield (Table 1). From Table 1, it is evident that all the compounds were moderate to highly fluorescent, and among them, compound **17a** showed the highest quantum yield (Φ_f) of 0.003.

Solubility, lipophilicity and conductivity study

Equilibrium between the hydrophilicity and lipophilicity is highly necessary to maintain the tumour-inhibiting potential of metal complexes. These Ru(II)-arene complexes were highly soluble in DMSO, DMF and have moderate to good solubility in H₂O, MeOH, EtOH and CH₃CN and poor solubility in hydro-

Table 1 Selected physico-chemical data of the synthesized organoruthenium complexes (**16a–b**, **17a–d** and **19a–c**)

Samples	λ_{\max}^a (nm)	λ_f^b (nm)	Stoke's shift	Peak area	OD ^c	ϵ^d (M ⁻¹ cm ⁻¹)	$(\phi_f)^e$	Solubility ^f (M)	log P ^g	Λ_M^h	
										DMSO 10%	aq DMSO
16a	336	432	96	434.182	0.70	23 333	0.0005	0.026	0.89 ± 0.03	65	162
16b	304	438	134	920.323	0.569	18 966	0.0013	0.024	1.10 ± 0.09	60	160
17a	354	440	86	1544.612	0.44	14 666	0.003	0.016	0.92 ± 0.06	25	92
17b	356	442	86	1137.83	0.27	9000	0.003	0.018	0.94 ± 0.07	27	94
17c	360	442	82	664.172	0.263	8766	0.002	0.012	0.88 ± 0.08	25	95
17d	340	434	94	831.862	0.21	7000	0.003	0.019	0.82 ± 0.02	28	96
19a	342	442	100	545.378	0.165	5500	0.003	0.029	0.49 ± 0.06	28	84
19b	344	436	92	369.054	0.405	13 500	0.0007	0.026	0.79 ± 0.03	32	86
19c	344	440	96	685.346	0.267	8900	0.002	0.025	0.78 ± 0.08	30	86
Quinine sulphate	350	452	102	56 001	0.07	—	0.564	—	—	—	—

^a Absorption maxima. ^b Emission wavelength. ^c Optical density. ^d Extinction coefficient. ^e Quantum yield. ^f DMSO-10% DMEM medium (1 : 99 v/v, comparable to cell media). ^g *n*-Octanol/water partition coefficient. ^h Conductance in DMSO and 10% aqueous DMSO.

carbon solvents. These complexes were soluble in the range of 5–10 mg per ml of DMSO-10% DMEM medium (1 : 99 v/v, comparable to cell media) at 25 °C, which is essential for delivering the drug into the target. The lipophilicity of these complexes was measured by an *n*-octanol/water partition coefficient ($\log P$) study.⁵⁸ To compare the lipophilic properties of the ruthenium complexes (**16a–b**, **17a–d**, **19a–c**), we estimated the *n*-octanol/water partition coefficient ($\log P$) using the shake flask method (Table 1). The experimental $\log P$ values of the complexes were obtained in the range 0.49–1.1. Complex **16b** exhibited the highest order of $\log P$ due to the lipophilic nature of its methyl group. The lowest order of $\log P$ value was observed in compound **19a** due to presence of hydrophilic –OH groups. The ruthenium complexes **17a–d** and **19a–c** exhibited the molar conductance values of ~ 25 – $30 \text{ S m}^2 \text{ M}^{-1}$ in pure DMSO. While, complexes **16a–b** displayed a greater conductance (~ 60 – $65 \text{ S m}^2 \text{ M}^{-1}$) in DMSO. The molar conductance of all these complexes were drastically increased in 10% aqueous DMSO (~ 80 – $160 \text{ S m}^2 \text{ M}^{-1}$, Table 1), suggesting their 1:1 electrolytic nature in both media due to the charged ruthenium ions.⁵⁹ The significant change in conductance in aqueous and non-aqueous media suggests a high rate of dissociation of chloride ligands from the ruthenium(II) complex. Moreover, the conductance value increased gradually with time (Table S1†). It is noteworthy that at lower pH, the conductance values of the complexes steadily increased (Table S2†). Similar results were also observed in higher DNA and GSH concentrations (Tables S3 and S4†). All these results sufficiently supported the DNA covalent interaction through aqua complex formation in a cancerous environment (low PH, high GSH).

Stability study of the complexes by UV-Vis spectroscopy

The stabilities of the three complexes, namely **16b**, **17a** and **19b**, were tested in 1% DMSO-PBS medium in order to assess them as a potent therapeutic agent, as the complexes need to be stable in the biological environment of cell. These complexes were found to be fairly stable in DMSO-buffer system from 0 h to the 48th h. There was no significant change in the spectral pattern, as shown in Fig. S2,† which suggests the stability of the complexes in MTT solvent and indicates they can be used for various cellular activities.

DNA binding study

Electronic absorption spectral studies. DNA is one of the most crucial pharmacological targets for various FDA-approved anticancer metallodrugs, like carboplatin, cisplatin, oxliplatin and organic drugs (doxorubicin, gemcitabine, 5-fluorouracil, *etc.*).⁶⁰ Various photophysical properties and structural diversities make these metal complexes good for use as DNA footprinting agents, molecular light-switches, sensors, and charge transfer agents, as well as useful for the site-specific recognition of DNA, and as diagnostic probes and for use in therapeutics.^{61,62} Therefore, the interaction of metal complexes with DNA is an effective strategy for designing effective chemotherapeutic drugs. Electronic absorption titration is the

most widely using method to identify this type of interaction. Here, we selected three different types of Ru(II)–arene complexes (**16b**, **17a** and **19b**) for measuring the CT-DNA binding strength, which was performed by electronic absorption titration and ethidium bromide displacement assay.

The λ_{max} values of the complexes **16b**, **17a** and **19b** were observed at 291, 292 and 288 nm respectively, while the λ_{max} of CT-DNA alone appeared at 258 nm. A decrease in wavelength (*i.e.*, hypsochromic shift) was observed (Fig. S3†) upon the first addition of CT-DNA to the complex solution. We also observed an increase in absorbance (*i.e.* hyperchromism) upon increasing CT-DNA addition to the metal complex. The binding constant (K_{b}) values calculated from eqn (i) were 4.4×10^3 , 3.49×10^3 and $5.5 \times 10^3 \text{ M}^{-1}$ for **16b**, **17a** and **19b**, respectively (Fig. S4,† and Table 2). These high binding constant values and significant hyperchromism in absorbance and the hypsochromic shift in wavelength after each addition of CT-DNA indicated an electrostatic mode of binding for these complexes with DNA.

Ethidium bromide (EtBr) binding study. The addition of Ru(II) complexes **16b**, **17a** and **19b** in the EtBr-CT-DNA adduct caused a decrease in fluorescence intensity (Fig. S5†) as the complexes displaced EtBr from the CT-DNA grooves so that the complexes themselves bound to the DNA base pairs. The excitation wavelengths for the EtBr-bound DNA and complexes **16b**, **17a** and **19b** were at 485 nm and the recorded emission wavelengths were at 600 nm. The concentrations of DNA and EtBr were 120 and 8 μM , respectively. The calculated value of K_{app} for the complexes were observed as $K_{\text{app}} = 2.6 \times 10^6 \text{ M}^{-1}$ (eqn (iii), Table 2). The value of K_{EtBr} found from literature was $1 \times 10^7 \text{ M}^{-1}$. The Stern–Volmer quenching constant (K_{SV}) values calculated from eqn (iv) for complexes **16b**, **17a** and **19b** were 0.04×10^5 , 0.01×10^5 and $0.1 \times 10^5 \text{ M}^{-1}$, respectively (Table 2).

Viscosity measurements. In order to find out the binding mode of drugs with DNA, a hydrodynamic method, like a viscosity study, needed to be conducted. Binding *via* intercalation requires the adjacent base pairs separation by allowing the drug molecules to enter into the DNA double helix, which leads to an increase in the length of DNA and their viscosity. The interaction of a drug *via* groove binding or electrostatic interaction does not change the relative viscosity of DNA, as the molecule does not change the length of DNA upon

Table 2 Binding parameters for the interaction of complexes **16b**, **17a** and **19b** with CT-DNA

Complex	$K_{\text{b}}^a \text{ (M}^{-1}\text{)}$	$K_{\text{SV}}^b \text{ (M}^{-1}\text{)}$	$K_{\text{app}}^c \text{ (M}^{-1}\text{)}$
16b	4.4×10^3	0.04×10^5	2.7×10^6
17a	3.49×10^3	0.01×10^5	2.4×10^6
19b	5.5×10^3	0.1×10^5	2.0×10^6

^a K_{b} , intrinsic DNA binding constant from UV-visible absorption titration. ^b K_{SV} , Stern–Volmer quenching constant. ^c K_{app} , apparent DNA binding constant from competitive displacement from fluorescence spectroscopy.

binding. A partial or non-classical intercalation of the compounds can bend or kink DNA, resulting in a decrease in its effective length, with a concomitant decrease in its viscosity. When a molecule binds covalently to DNA, it results in an unwinding and bending of the DNA double helix. This results in a decrease in the effective length of DNA, which ultimately decreases the relative viscosity of DNA solution. The viscosity study of our prepared complex (**16b**) showed that initially, up to 10 μM concentration, it exhibited a strong intercalative capability towards DNA, which was evident from the steady increase of viscosity from 0–10 μM concentration, and after that it showed a decent intercalation with DNA molecules up to 50 μM concentration, marked by the slow increase of viscosity with the increase in complex concentration (Fig. S6†). However, with a gradual increase in concentration after 50 μM onwards, this drug dramatically modified itself as a good electrostatic or groove binder to DNA which was apparent from the line parallel to the X-axis in the viscosity graph. Again, if we cast our vision beyond a 10 μM concentration, it is clear that the drug binds to the DNA base pair covalently with the gradual decrease in complex concentration, which could be confirmed by the steady decrease in viscosity, which was also consistent with the study of the conductance in the presence of DNA, whereby the conductance increases with the gradual decrease in r_i value, indicating the covalent binding nature of the complex. From that point of view, we can say that our justification perfectly fitted with all the experimental results, ensuring the possibility of the binding ability of all our metal complexes with DNA through different modes.

BSA binding study. The gradual decrease in fluorescence intensity (Fig. S7†) with the subsequent increase in concentrations of **16b**, **17a** and **19b** confirmed the binding of the complexes with BSA. The excitation wavelength used for this titration study was 295 nm, while the emission was observed at 350 nm. The Stern–Volmer quenching constant for BSA fluorescence (K_{BSA}), calculated using eqn (v), was found to be 0.58×10^6 , 0.26×10^6 and $2.0 \times 10^6 \text{ M}^{-1}$ for **16b**, **17a** and **19b**, respectively (Fig. S8†). The highest value of K_{BSA} of compound **19b** among the other two is due to the presence of polar groups, like OH, which aid its binding with the polar amino acids of BSA. Scatchard plot analysis gave binding affinity (K) values for **16b**, **17a** and **19b** of 8.74×10^3 , 4.39×10^3 and $32.7 \times 10^3 \text{ M}^{-1}$, respectively (eqn (vi), Fig. S9†). These high binding constant values confirm the occurrence of strong interactions among BSA and ruthenium complexes, which is essential for transport of the complexes across the biological system. The number of sites (n) that BSA can make available to bind complexes **16b**, **17a** and **19b** was found to be 0.9, 0.82 and 0.698, respectively (Table 3).

Cytotoxic activity. Cytotoxicity study of all the synthesized Ru(II)-arene complexes (**16a–b**, **17a–d**, **19a–c**) was performed via a typical 3-(4,5-dimethylthiazol-2-yl)-2,5-diphenyltetrazolium bromide (MTT) assay protocol together with a panel of cancer cell lines, i.e. colorectal adenocarcinoma cells (Caco-2), human epitheloid cervix carcinoma (HeLa), and one normal cell line, i.e. human embryonic kidney cells (HEK-293) in tripli-

Table 3 Binding parameters for the interaction of complexes **16b**, **17a** and **19b** with BSA

Complex	$K_{\text{BSA}}^a (\text{M}^{-1})$	$K_q^b (\text{M}^{-1} \text{ s}^{-1})$	$K^c (\text{M}^{-1})$	n^d
16b	0.58×10^6	0.58×10^{14}	8.74×10^3	0.90
17a	0.26×10^6	0.26×10^{14}	4.39×10^3	0.82
19b	2.01×10^6	2.01×10^{14}	32.7×10^3	0.698

^a K_{BSA} , Stern–Volmer quenching constant. ^b K_q , quenching rate constant. ^c K , binding constant with BSA. ^d n , number of binding sites.

Table 4 MTT cytotoxicity screening of Ru(II)-arene complexes (**16a–b**, **17a–d**, **19a–c**) at 24 h of drug exposure

Compounds	IC ₅₀ (μM) ^a				SF ^b
	HeLa ^c	Caco-2 ^c	HEK-293	HeLa	
16a	6.7 ± 0.7	11.8 ± 0.6	>100	>14.9	>8.4
16b	1.2 ± 0.9	9.0 ± 0.4	>100	>83.3	>11.1
17a	3.4 ± 0.8	9.1 ± 0.8	>100	>29.4	>10.9
17b	17.6 ± 1.4	13.4 ± 0.9	>100	>5.7	>7.4
17c	3.2 ± 0.5	9.1 ± 0.6	>100	>31.2	>11.1
17d	15.3 ± 1.6	26.8 ± 1.2	>100	>6.5	>3.7
19a	>100	29.2 ± 1.1	>100	—	8.74
19b	4.2 ± 0.8	12.8 ± 0.9	>100	>23.8	>7.8
19c	3.1 ± 1.2	11.1 ± 1.1	>100	>32.2	>9.0
DMSO	—	—	—	—	—
CisPlatin	20 ± 0.8	11 ± 0.6	32.2 ± 1.8	1.61	2.93
RAPTA-C	16.2 ± 0.5	11.9 ± 0.8	55.2 ± 1.2	3.40	5.17

^a IC₅₀ is the concentration at which 50% of cells undergo cytotoxic cell death due to organoruthenium or cisplatin treatment. ^b SF (selectivity factor) = ratio of IC₅₀ for HEK-293 and IC₅₀ for all the cancer cell lines. HEK-293 fibroblasts are generally selected as the model for healthy cells in the evaluation of chemotherapeutic drug selectivity. ^c 24 h incubation time for the HeLa and Caco-2 cell lines.

cate. The cells were treated with these ruthenium complexes along with cisplatin and RAPTA-C as the standard positive control with variable concentrations (0–200 μM) for 24 h. Most of the ruthenium complexes exhibited higher potency in HeLa and Caco-2 cell lines than cisplatin and RAPTA-C (Table 4). It was noteworthy that the majority of the compounds were 3–83-fold more selective with cancer cells (HeLa, Caco-2) than with normal human embryonic kidney cells (HEK-293). Nevertheless, cisplatin and RAPTA-C exhibited insignificant cytotoxicity with those cancer cell lines. Among the synthesized ruthenium complexes, compound **16b** presented the greatest potency and selectivity with both cell lines.

Structure–activity relationship (SAR) study. Ru(II)-*p*-cymene imidazophenanthroline complexes displayed excellent potency in both cancer cell lines with high selectivity (Fig. 4).

These types of ruthenium complexes having planner imidazophenanthroline ligands induce cancer cell apoptosis via an effective DNA intercalation. The methyl group attached to the *para* position of biphenyl imidazophenanthroline ligands enhanced the selective cellular uptake of complex **16b** in cancer cells, which induced apoptosis via DNA intercalation.

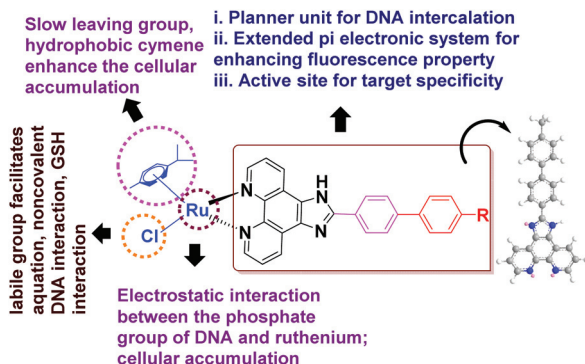


Fig. 4 SAR of Ru(II)-arene imidazophenanthroline complexes.

However, the ruthenium complexes having ((ethynyl)phenyl)-1*H*-imidazo[4,5-*f*][1,10]phenanthroline ligands (**17a–d**) displayed lower efficacy than complex **16b**. This is because of the slightly non-planner nature of their ligands. Among these four scaffolds, complexes **17a** and **17c** showed comparable efficacy with complex **16b**. After introducing benzene 1,3 diol at the 2-position of the imidazophenanthroline ligand, the potency of complex **19a** was drastically reduced because of the presence of two hydrophilic –OH groups. However, compounds **19b** and **19c** showed significant cytoselectivity with both cancer cells more than with normal cells. The lipophilic methyl and methoxy groups of these complexes increase the cellular accumulation. The presence of one –OH group also facilitates the interaction with BSA followed by drug transportation.

Live-cell-imaging study. We performed cellular imaging experiments using the HeLa cell line. The cells were incubated for different times (30 min, 1 h, 2 h) at 37 °C with complex **17a**

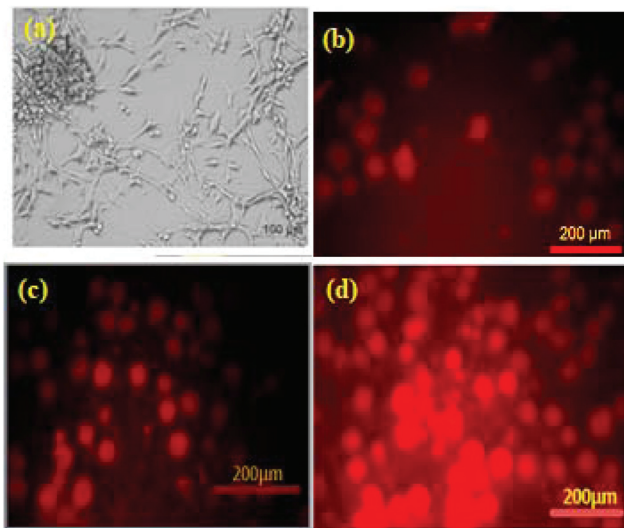


Fig. 5 Fluorescence images of live HeLa cells with compound **17a** (a) and control HeLa cell without drug in bright field; (b) **17a** + cell under green filter [50 μM in PBS buffer; incubation time 30 min] (c) **17a** + cell in green filter [50 μM in PBS buffer; incubation time 1 h]; (d) **17a** + cell in green filter [50 μM in PBS buffer; incubation time 2 h] Scale bar 200 μm.

(50 μM). After 2 h of incubation, the complex-treated cells were excited through a 450–500 nm excitation filter for fluorescence microscopy analysis. Live cells were tracked by the red fluorescence of the compounds under a fluorescence microscope (Fig. 5). These imaging results represent clear evidence of the strong cellular uptake of complex **17a** at 2 h incubation in the HeLa cell line compared to a lesser time of incubation.

Experimental section

Materials and methods

All the reagents and solvents used had the highest commercial quality. Organic solvents used for the chemical synthesis and for chromatography were acquired from E. Merck (India) and were of analytical grade. Dichloro-*p*-cymene ruthenium(II) chloride, 1,10-phenanthroline-5,6-dione, 4-bromobenzaldehyde, organoboronic acids, phenyl acetylene and its derivatives, 2,4-dihydroxybenzaldehyde, 2-hydroxy-4-methylbenzaldehyde, 2-hydroxy-4-methoxybenzaldehyde and tetrakis (triphenylphosphine)palladium(0) were purchased from Sigma Aldrich Chemical Ltd, Merck and Spectrochem. Microwave reactions were performed in catalytic systems. HeLa and HEK-293 cell lines were purchased from NCCS, Pune. The Caco-2 cell line was procured from ATCC. CT-DNA and BSA were purchased from Sigma Aldrich Chemical Ltd. ¹H NMR, ¹³C NMR, ¹⁹F NMR and ³¹P NMR spectra were recorded on a Bruker DPX spectrometer at 400 MHz with tetramethylsilane as the internal standard and the chemical shifts has been reported herein in ppm units. The melting points of the complexes were measured on an Elchem Microprocessor DT apparatus using an open capillary tube and are uncorrected herein. The synthesized compounds were also characterized using a Shimadzu LCMS-4000 LC-MS instrument, having 4000 triple quadrupole MS, using methanol as the solvent. TLC was performed on pre-coated silica gel 60 F₂₅₄ aluminium sheets (E. Merck, Germany) using methanol/ethyl acetate mixture as the solvent system. UV-Visible spectra were recorded on a JASCO V-730 spectrometer and fluorescence measurements were carried out using an HITACHI fluorescence spectrophotometer equipped with a xenon lamp. An Elisa reader and 96-well plates were used for the MTT assay. The fluorescence imaging study was performed using an Olympus model CKX41 microscope.

Synthetic procedure of 2-(4-bromophenyl)-1*H*-Imidazo[4,5-*f*][1,10]phenanthroline (**10**)

First, 500 mg (2.380 mmol) of 1,10-phenanthroline-5,6-dione (**8**) was taken in a 50 ml round-bottom flask followed by the addition of 484 mg (2.617 mmol, 1.1 equiv.) of 4-bromobenzaldehyde (**9**) and 1.46 g (19.03 mmol, 8 equiv.) of ammonium acetate. All the reagents were dissolved in 10 ml of glacial acetic acid and the mixture was kept in reflux for 24 h. TLC was monitored to observe the change in the reaction mixture. As soon as the reaction was over, the reaction mixture was poured into ice cold water and concentrated ammonia was

added to neutralize the solution. Then, the above-neutralized solution was allowed to settle for 30 min and was then filtered. The yellowish–orange product was dried and recrystallized from ethyl acetate in a high yield (~96%).

2-(4-Bromophenyl)-1*H*-imidazo[4,5-*f*][1,10]phenanthroline (10). Yield: 96%; m.p: 250–252 °C; R_f : 0.54 (ethyl acetate : methanol in 3 : 1); ^1H NMR (DMSO- d_6 , 400 MHz): δ 7.78–7.83 (m, 4H, ArH), 8.23 (d, 2H, J = 8 Hz, ArH), 8.91 (d, 2H, J = 8 Hz, ArH), 9.01 (d, 2H, J = 4 Hz, ArH); ^{13}C (DMSO- d_6 , 100 MHz): δ 122.0 (CH), 123.3 (C), 123.8 (C), 128.6 (C), 129.8 (CH), 130.2 (CH), 131.7 (CH), 132.4 (C), 143.9 (CH), 148.2 (C), 150.2 (C); IR (cm $^{-1}$): ν sp 2 C–H stretching (3176), Arm C–H stretching (3026), N–H bending (1664), Arm C=C stretching (1400), C–N stretching (1352), C–H bending (719), C–Br stretching (619); LCMS (MeOH): m/z : 375.2 [M + H] $^+$.

Synthesis of biphenyl imidazo[4,5-*f*][1,10]phenanthroline (12a–b)

First, 50 mg (0.133 mmol) of compound 2-(4-bromophenyl)-1*H*-imidazo[4,5-*f*][1,10]phenanthroline (**10**), 1.3 equivalent of aryl boronic acid (**11a–b**), 0.5 mol% of (PPh $_3$) $_4$ Pd, 20 mol% of NaOH in water and 4 mL of DMF were taken in a microwave flask. Microwave-assisted reaction was performed for 15 min, at 450 W and a temperature of 150 °C. The completion of the reaction was marked by a colour change of the reaction mixture from orange to dark brown. TLC was monitored to confirm the completion of the reaction. The mixture was then poured into a crushed-ice medium followed by extraction with ethyl acetate using a separating funnel. Then, the organic layer (*i.e.* ethyl acetate) was separated and the water layer was drained off. After 4–5 times washing, the organic layers were collected and dried with anhydrous sodium sulphate and the solvent was evaporated using a rotary evaporator. The dried product was washed with hexane followed by recrystallization from ethyl acetate. Finally, brown needle-shaped crystals of compounds **12a–b** were obtained in high yields (~85–90%).

2-([1,1'-Biphenyl]-4-yl)-1*H*-imidazo[4,5-*f*][1,10]phenanthroline (12a). Yield: 85%; m.p: 175–177 °C; R_f : 0.7 (ethyl acetate : methanol = 1 : 1); ^1H NMR (DMSO- d_6 , 400 MHz): δ 7.43 (s, 1H, ArH), 7.50 (t, 2H, J = 8 Hz, ArH), 7.78 (d, 2H, J = 8 Hz, ArH), 7.84 (t, 2H, J = 4 Hz, ArH), 7.91 (d, 2H, J = 8 Hz, ArH), 8.38 (d, 2H, J = 8 Hz, ArH), 8.96 (d, 2H, J = 8 Hz, ArH), 9.02 (brs, 2H, ArH); ^{13}C (DMSO- d_6 , 100 MHz): δ 123.8 (CH), 127.1 (C), 127.3 (C), 127.6 (C), 127.6 (C), 127.8 (CH), 128.4 (CH), 129.1 (CH), 129.4 (CH), 129.5 (CH), 129.6 (CH), 130.2 (C), 130.6 (C), 139.7 (C), 141.5 (C), 143.9 (CH), 148.3 (C), 150.9 (C); IR (cm $^{-1}$): ν Arm C–H stretching (3032), N–H bending (1664), Arm C=C stretching (1400), C–N stretching (1072), C–H bending (732); LCMS (MeOH): m/z : 373.1 [M + H] $^+$.

2-(4'-Methyl-[1,1'-biphenyl]-4-yl)-1*H*-imidazo[4,5-*f*][1,10]phenanthroline (12b). Yield: 90%; m.p: 192–194 °C; R_f : 0.62 (ethyl acetate : methanol = 1 : 1); ^1H NMR (DMSO- d_6 , 400 MHz): δ 2.37 (s, 3H, CH $_3$), 7.33 (d, 2H, J = 8 Hz, ArH), 7.69 (d, 2H, J = 8 Hz, ArH), 7.85 (m, 2H, ArH), 7.91 (d, 2H, J = 8 Hz, ArH), 8.37 (d, 2H, J = 8 Hz, ArH), 8.96 (d, 2H, J = 8 Hz, ArH), 9.05 (d, 2H, J = 4 Hz, ArH); IR (cm $^{-1}$): ν Arm C–H stretching (3061), N–H

bending (1571), Arm C=C stretching (1477), sp 3 C–H bending (1448), C–N stretching (1352), C–H bending (736).

Synthesis of ((phenylethynyl)phenyl)imidazo[4,5-*f*][1,10]phenanthroline analogues (14a–d)

First, 50 mg (0.133 mmol) of compound 2-(4-bromophenyl)-1*H*-imidazo[4,5-*f*][1,10]phenanthroline (**10**), 2 equivalent of phenylacetylene derivatives (**13a–d**), 0.5 mol% of (PPh $_3$) $_4$ Pd, 20 mol% of NaOH and 4 ml of DMF were taken in a microwave flask. Microwave-assisted reaction was performed for 15 min, at 450 W and a temperature of 150 °C. The completion of the reaction was marked by a colour change of the reaction mixture from yellow to dark brown. TLC was monitored to confirm the completion of the reaction. The mixture was then poured into a crushed-ice medium followed by extraction with ethyl acetate using a separating funnel. After 4–5 times washing, all the organic layers were collected and dried with anhydrous sodium sulphate and the solvent was evaporated using a rotary evaporator. The dried product was washed with hexane followed by recrystallization from ethyl acetate. Finally, dark yellow needle-like crystals of compounds **14a–d** were obtained in high yields (~90–95%).

2-(4-(Phenylethynyl)phenyl)-1*H*-imidazo[4,5-*f*][1,10]phenanthroline (14a). Yield: 90%; m.p: 200–220 °C; R_f : 0.59 (ethyl acetate : methanol in 1 : 1); ^1H NMR (DMSO- d_6 , 400 MHz): δ 7.46 (d, 2H, J = 8 Hz, ArH), 7.58 (m, 4H, ArH), 7.70 (d, 1H, J = 8 Hz, ArH), 7.80 (t, 2H, J = 4 Hz, ArH), 8.42 (d, 1H, J = 8 Hz, ArH), 8.58 (s, 1H, ArH), 8.98 (m, 4H, ArH); ^{13}C (DMSO- d_6 , 400 MHz): δ 123.5 (CH), 126.8 (C), 129.2 (C), 129.3 (CH), 130.3 (CH), 131.9 (C), 131.9 (CH), 132.0 (C), 132.2 (C); IR (cm $^{-1}$): ν sp C–H stretching (3298), N–H bending (1583), Arm C=C stretching (1479), C–N stretching (1348), C–H bending (738).

2-(4-(*p*-Tolyethynyl)phenyl)-1*H*-imidazo[4,5-*f*][1,10]phenanthroline (14b). Yield: 92%; m.p: 185–187 °C; R_f : 0.52 (ethyl acetate : methanol in 1 : 1); ^1H NMR (DMSO- d_6 , 400 MHz): δ 2.29 (s, 3H, CH $_3$), 7.22 (d, 2H, J = 8 Hz, ArH), 7.33 (d, 2H, J = 8 Hz, ArH), 7.72 (m, 4H, ArH), 8.23 (d, 1H, J = 8 Hz, ArH), 8.36 (d, 1H, J = 8 Hz, ArH), 8.89 (d, 4H, J = 4 Hz, ArH); ^{13}C (DMSO- d_6 , 100 MHz): δ 123.3 (CH), 129.0 (C), 129.2 (C), 129.3 (CH), 129.4 (CH), 130.1 (C), 131.9 (CH), 132.0 (C); IR (cm $^{-1}$): ν N–H stretching (3317), sp 3 C–H stretching (2922), N–H bending (1658), Arm C=C stretching (1438), C–N stretching (1352), C–H bending (696).

2-(4-((4-Methoxyphenyl)ethynyl)phenyl)-1*H*-imidazo[4,5-*f*][1,10]phenanthroline (14c). Yield: 93%; m.p: 180–182 °C; R_f : 0.64 (ethyl acetate : methanol in 1 : 1); ^1H NMR (DMSO- d_6 , 400 MHz): δ 3.78 (s, 3H, OCH $_3$), 7.23 (d, 1H, J = 8 Hz, ArH), 7.43 (d, 1H, J = 8 Hz, ArH), 7.59 (m, 4H, ArH), 7.83 (t, 2H, J = 4 Hz, ArH), 8.20 (d, 1H, J = 8 Hz, ArH), 8.32 (d, 1H, J = 8 Hz, ArH), 8.98 (m, 4H, ArH); ^{13}C (DMSO- d_6 , 400 MHz): δ 55.6 (OCH $_3$), 114.3 (CH), 123.8 (C), 126.7 (CH), 126.8 (C), 129.2 (C), 129.3 (C), 129.4 (CH), 130.4 (CH), 130.4 (CH), 131.8 (C), 131.9 (CH), 132.6 (C), 143.7 (C), 148.2 (C); IR (cm $^{-1}$): ν N–H stretching (3280), sp 3 C–H stretching (2931), N–H bending (1600), Arm C=C stretching (1444), C–N stretching (1350), C–O stretching (1247), C–H bending (736).

2-(4-(Pyridin-2-ylethynyl)phenyl)-1H-imidazo[4,5-f][1,10]phenanthroline (14d). Yield: 95%; m.p: 168–170 °C; R_f : 0.42 (ethyl acetate : methanol in 1 : 1); ^1H NMR (DMSO- d_6 , 400 MHz): δ 7.62–7.65 (m, 2H, ArH), 7.71 (d, 1H, J = 8 Hz, ArH), 7.87 (d, 4H, J = 8 Hz, ArH), 8.38 (d, 2H, J = 8 Hz, ArH), 8.65 (d, 1H, J = 4 Hz, ArH), 8.95 (d, 2H, J = 8 Hz, ArH), 9.05 (d, 2H, J = 4 Hz, ArH); ^{13}C (DMSO- d_6 , 400 MHz): δ 126.9 (CH), 127.9 (CH), 129.2 (CH), 129.3 (C), 131.9 (C), 132.0 (CH), 132.5 (C), 132.9 (C); IR (cm $^{-1}$): ν N–H stretching (3346), Arm C–H stretching (3059), C=C stretching (2216), N–H bending (1581), Arm C=C stretching (1431), C–N stretching (1348), C–H bending (738).

Synthesis of (imidazo[4,5-f][1,10]phenanthroline-2-yl) phenol analogues (18a–c)

First, 50 mg (0.238 mmol) of 1,10-phenanthroline-5,6-dione (**8**) was taken in a 25 ml round-bottom flask and 1.1 equivalent of 2-hydroxybenzaldehyde derivatives (**17a–c**) was added followed by 147 mg (1.903 mmol, 8 equiv.) of ammonium acetate. The reagents were dissolved in 5 ml of glacial acetic acid and kept in reflux for 24 h. TLC was monitored to observe the change in the reaction. As soon as the reaction was completed, the reaction mixture was poured in ice-cold water and concentrated ammonia was added in drops to neutralize the solution. Then, the above neutralized solution was allowed to settle for 30 min. The precipitate formed was then filtered. The products **18a–c** were dried and recrystallized from ethyl acetate in high yields (~96–97%).

4-(1H-Imidazo[4,5-f][1,10]phenanthroline-2-yl)benzene-1,3-diol (18a). Yield: 96%; m.p: 224–226 °C; R_f : 0.35 (ethyl acetate : methanol in 1 : 1); ^1H NMR (DMSO- d_6 , 400 MHz): δ 6.46 (s, 1H, ArH), 6.50 (d, 1H, J = 8 Hz, ArH), 7.82 (m, 2H, ArH), 7.99 (d, 1H, J = 8 Hz, ArH), 8.88 (d, 2H, J = 8 Hz, ArH), 9.02 (d, 2H, J = 4 Hz, ArH); ^{13}C (DMSO- d_6 , 400 MHz): solubility problem; IR (cm $^{-1}$): ν sp 2 C–H stretching (3062), Arm C–H stretching (2978), N–H bending (1627), Arm C=C stretching (1477), O–H bending (1404), C–N stretching (1253), C–O stretching (1066), C–H bending (736).

2-(1H-Imidazo[4,5-f][1,10]phenanthroline-2-yl)-5-methylphenol (18b). Yield: 97%; m.p: 190–192 °C; R_f : 0.85 (ethyl acetate : methanol in 1 : 1); ^1H NMR (DMSO- d_6 , 400 MHz): δ 2.31 (s, 3H, CH $_3$), 6.79 (d, 2H, J = 16 Hz, ArH), 7.77 (d, 2H, J = 4 Hz, ArH), 8.08 (d, 1H, J = 8 Hz, ArH), 8.87 (d, 2H, J = 8 Hz, ArH), 8.98 (d, 2H, J = 4 Hz, ArH), 9.10 (s, 1H, OH); ^{13}C (DMSO- d_6 , 100 MHz): δ 21.6 (CH $_3$), 117.6 (CH), 123.6 (CH), 124.4 (CH), 126.3 (CH), 130.1 (C), 131.0 (C), 147.7 (C); IR (cm $^{-1}$): ν Arm C–H stretching (2920), sp 3 C–H stretching (2849), O–H stretching (2743), N–H bending (1635), Arm C=C stretching (1550), O–H bending (1400), C–N stretching (1355), C–O stretching (1066), C–H bending (734).

2-(1H-Imidazo[4,5-f][1,10]phenanthroline-2-yl)-5-methoxyphenol (18c). Yield: 96%; m.p: 182–184 °C; R_f : 0.5 (ethyl acetate : methanol in 1 : 1); ^1H NMR (DMSO- d_6 , 400 MHz): δ 3.84 (s, 3H, OCH $_3$), 6.59 (s, 1H, ArH), 6.65 (d, 1H, J = 4 Hz, ArH), 7.78 (m, 2H, ArH), 8.07 (d, 1H, J = 8 Hz, ArH), 8.84 (d, 2H, J = 12 Hz, ArH), 8.99 (d, 2H, J = 4 Hz, ArH), 9.09 (s, 1H, OH); ^{13}C (DMSO- d_6 , 400 MHz): δ 55.8 (OCH $_3$), 101.9 (CH), 106.8 (C), 107.0 (CH),

123.7 (C), 124.2 (C), 127.5 (CH), 130.1 (CH), 143.8 (CH), 148.2 (C), 151.9 (C), 159.6 (C), 162.2 (C); IR (cm $^{-1}$): ν O–H stretching (3180), Arm C–H stretching (3061), sp 3 C–H stretching (2933), N–H bending (1631), Arm C=C stretching (1589), O–H bending (1481), C–N stretching (1386), C–O stretching (1261), C–H bending (734).

Synthesis of $[(\eta^6\text{-}p\text{-cymene})\text{RuCl}(\text{K}^2\text{-}N,N\text{-}2\text{-}(\text{biphenyl})\text{-}1\text{H}\text{-imidazo}[4,5\text{-}f][1,10]\text{phenanthroline})]\text{-PF}_6$ analogues (16a–b)

First, 20 mg (0.033 mmol) of dichloro(*p*-cymene)ruthenium(II) dimer (**15**) was dissolved in 7 ml of methanol in a 50 ml round-bottom flask and stirred for 10 min to dissolve the compound in methanol. Thereafter, 2.1 equivalent of the previously prepared ligand **12a,b** (**12a**: 25.8 mg, **12b**: 26.78 mg) was added to the reaction mixture followed by magnetic stirring for another 2 h. A change in colour occurred from deep yellow to deep orange. Then, 13 mg (0.082 mmol, 2.5 equiv.) of NH $_4$ PF $_6$ was added to the reaction mixture and stirred for another 1 h. The reaction was monitored by TLC using 100% methanol as the solvent system. After completion of the reaction, the methanol was evaporated off using a rotary evaporator and the crude product was further recrystallized from a diethyl ether/methanol mixture. Orange fine crystals of **16a–b** were isolated in high yields (~96–97%).

$[(\eta^6\text{-}p\text{-Cymene})\text{RuCl}(\text{K}^2\text{-}N,N\text{-}2\text{-}([1,1'\text{-biphenyl}]\text{-}4\text{-yl})\text{-}1\text{H}\text{-imidazo}[4,5\text{-}f][1,10]\text{phenanthroline})]\text{-PF}_6$ (**16a**). Yield: 49.9 mg (0.0634 mmol, 97%). Mr (C $_{35}$ H $_{30}$ N $_4$ ClF $_6$ PRu) = 788.13 g mol $^{-1}$. Anal. Calcd for C $_{35}$ H $_{30}$ N $_4$ ClF $_6$ PRu: C 53.34, H 3.84, N 7.11; found: C 53.06; H 3.44; N 7.40; m.p: 164–166 °C; R_f (100% methanol): 0.52; ^1H NMR (DMSO- d_6 , 400 MHz): δ 0.89 (d, 6H, J = 8 Hz, cymene isopropyl-CH $_3$), 2.2 (s, 3H, cymene CH $_3$), 2.58–2.64 (m, 1H, cymene CH), 6.09 (d, 2H, J = 8 Hz, cymene ArH), 6.33 (d, 2H, J = 8 Hz, cymene ArH), 7.48 (t, 1H, ArH), 7.53 (d, 2H, J = 8 Hz, ArH), 7.80 (d, 2H, J = 8 Hz, ArH), 7.95 (d, 2H, J = 8 Hz, ArH), 8.20 (m, 2H, ArH), 8.43 (d, 2H, J = 8 Hz, ArH), 9.30 (d, 2H, J = 8 Hz, ArH), 9.84 (d, 2H, J = 4 Hz, ArH); ^{13}C NMR (DMSO- d_6 , 100 MHz): δ 18.3 (Me, *p*-cymene), 21.9 (Me, *p*-cymene), 22.1 (Me, *p*-cymene), 30.5 (CH, *p*-cymene), 84.4 (ArCH, *p*-cymene), 85.9 (ArCH, *p*-cymene), 86.7 (ArCH, *p*-cymene), 86.8 (ArCH, *p*-cymene), 100.6 (ArC, *p*-cymene), 103.6 (ArC, *p*-cymene), 106.9, 126.8, 127.2, 129.1, 129.7, 132.7, 133.0, 143.6, 154.4; ^{19}F NMR (DMSO- d_6 , 376 MHz): δ -71.03 (PF $_6$), -69.14 (PF $_6$); ^{31}P NMR (DMSO- d_6 , 162 MHz): δ -153.02 (PF $_6$), -148.64 (PF $_6$), -144.24 (PF $_6$), -139.85 (PF $_6$), -135.46 (PF $_6$); IR (cm $^{-1}$): ν N–H stretching (3369), Arm C–H stretching (3124), sp 3 C–H stretching (2924), N–H bending (1604), sp 3 C–H bending (1460), Arm C=C stretching (1406), C–N stretching (1199), P–F stretching (831), C–H bending (769); LCMS (MeOH): m/z : 643.3 [M] $^+$.

$[(\eta^6\text{-}p\text{-Cymene})\text{RuCl}(\text{K}^2\text{-}N,N\text{-}2\text{-}(4'\text{-methyl-[1,1'\text{-biphenyl}]}\text{-}4\text{-yl})\text{-}1\text{H}\text{-imidazo}[4,5\text{-}f][1,10]\text{phenanthroline})]\text{-PF}_6$ (**16b**). 50.3 mg (0.0627 mmol, 96%); Mr (C $_{36}$ H $_{32}$ N $_4$ ClF $_6$ PRu) = 802.15 g mol $^{-1}$; Anal. Calcd for C $_{36}$ H $_{32}$ N $_4$ ClF $_6$ PRu: C 53.90, H 4.02, N 6.98; Found: C 53.56; H 3.84; N 7.34; m.p: 170–172 °C; R_f (100% methanol): 0.67; ^1H NMR (DMSO- d_6 , 400 MHz): δ 0.90–0.92 (d, 6H, J = 8 Hz, cymene isopropyl-CH $_3$), 2.21 (s, 3H, cymene CH $_3$),

2.38 (s, 1H, CH₃, ligand), 2.58–2.64 (m, 1H, cymene CH), 6.11 (d, 2H, *J* = 8 Hz, cymene ArH), 6.34 (d, 2H, *J* = 8 Hz, cymene ArH), 7.34 (d, 2H, ArH), 7.71 (d, 2H, *J* = 8 Hz, ArH), 7.86 (d, 1H, *J* = 8 Hz, ArH), 7.95 (d, 1H, *J* = 8 Hz, ArH), 8.20–8.24 (m, 2H, ArH), 8.29–8.31 (d, 1H, *J* = 8 Hz, ArH), 8.42 (d, 1H, *J* = 8 Hz, ArH), 9.30 (d, 2H, *J* = 4 Hz, ArH), 9.86 (d, 2H, *J* = 4 Hz, ArH); ¹³C NMR (DMSO-*d*₆, 100 MHz): δ 18.8 (Me, *p*-cymene), 21.9 (Me, *p*-cymene), 22.0 (Me, *p*-cymene), 24.4 (Me, ligand), 30.9 (CH, *p*-cymene), 84.3 (ArCH, *p*-cymene), 85.9 (ArCH, *p*-cymene), 86.7 (ArCH, *p*-cymene), 86.8 (ArCH, *p*-cymene), 100.7 (ArC, *p*-cymene), 104.3 (ArC, *p*-cymene), 107.1, 126.6, 126.8, 127.0, 127.5, 127.7, 129.3, 129.7, 130.2, 132.9, 143.6, 154.2; ¹⁹F NMR (DMSO-*d*₆, 376 MHz): δ -71.07 (PF₆), -69.19 (PF₆); ³¹P NMR (DMSO-*d*₆, 162 MHz): δ -157.38 (PF₆), -152.98 (PF₆), -148.60 (PF₆), -144.20 (PF₆), -139.81 (PF₆), -135.43 (PF₆), -131.03 (PF₆); IR (cm⁻¹): ν sp² C–H stretching (3142), Arm C–H stretching (3049), sp³ C–H stretching (2968), N–H bending (1606), sp³ C–H bending (1450), Arm C=C stretching (1406), C–N stretching (1116), P–F stretching (831), C–H bending (721); LCMS (MeOH): *m/z*: 657.8 [M]⁺.

Synthesis of [(η⁶-*p*-cymene)RuCl(K²-*N,N*-2-(ethynyl)phenyl)-1*H*-imidazo[4,5-*f*][1,10]phenanthroline]-PF₆ analogues (17a–d)

First, 20 mg (0.033 mmol) of dichloro(*p*-cymene)ruthenium(II) dimer (15) was dissolved in 7 ml of methanol in a 50 ml round-bottom flask and stirred for 10 min to dissolve the compound in the methanol. Thereafter, 2.1 equivalent of the previously prepared ligand **14a–d** (**14a**: 27.5 mg, **14b**: 28.5 mg, **14c**: 29.5 mg, **14d**: 27.5 mg) was added to the reaction mixture followed by magnetic stirring for another 2 h. A change in colour occurred from deep yellow to brown. Then, 13 mg (0.082 mmol, 2.5 equiv.) of NH₄PF₆ was added to the reaction mixture and stirred for another 1 h. The reaction was monitored by TLC using 100% methanol as the solvent system. After completion of the reaction, the methanol was evaporated off using a rotary evaporator and the crude product was further recrystallized from a diethyl ether/methanol mixture. Orange fine crystals of **17a–d** were obtained in high yields (~96–98%).

[(η⁶-*p*-Cymene)RuCl(K²-*N,N*-2-(4-(phenylethynyl)phenyl)-1*H*-imidazo[4,5-*f*][1,10]phenanthroline)]-PF₆ (**17a**). 51.5 mg (0.0634 mmol, 97%); Mr (C₃₇H₃₀N₄ClF₆PRu) = 812.15 g mol⁻¹; Anal. Calcd for C₃₇H₃₀N₄ClF₆PRu: C 54.72, H 3.72, N 6.90; found: C 54.36; H 3.44; N 7.28; m.p.: 172–174 °C; *R*_f (100% methanol): 0.81; ¹H NMR (DMSO-*d*₆, 400 MHz): δ 0.89 (d, 6H, *J* = 8 Hz, cymene isopropyl-CH₃), 2.2 (s, 3H, cymene CH₃), 2.60–2.63 (m, 1H, cymene CH), 6.11 (d, 2H, *J* = 8 Hz, cymene ArH), 6.34 (d, 2H, *J* = 8 Hz, cymene ArH), 7.47 (d, 2H, *J* = 4 Hz, ArH), 7.62 (d, 4H, *J* = 4 Hz, ArH), 7.79 (d, 1H, *J* = 8 Hz, ArH), 8.19 (d, 2H, *J* = 4 Hz, ArH), 8.44 (d, 2H, *J* = 8 Hz, ArH), 9.29 (m, 2H, ArH), 9.82 (d, 2H, *J* = 8 Hz, ArH); ¹³C NMR (DMSO-*d*₆, 100 MHz): δ 18.3 (Me, *p*-cymene), 21.9 (Me, *p*-cymene), 22.1 (Me, *p*-cymene), 30.5 (CH, *p*-cymene), 82.3 (ArCH, *p*-cymene), 84.4 (ArCH, *p*-cymene), 85.9 (ArCH, *p*-cymene), 86.8 (ArCH, *p*-cymene), 96.9, 100.6 (ArC, *p*-cymene), 104.4 (ArC, *p*-cymene), 107.0, 126.8, 127.5, 129.3, 130.3, 131.0, 131.9, 133.0, 143.8,

154.4; ¹⁹F NMR (DMSO-*d*₆, 376 MHz): δ -71.08 (PF₆), -69.19 (PF₆); ³¹P NMR (DMSO-*d*₆, 162 MHz): δ -152.99 (PF₆), -148.60 (PF₆), -144.21 (PF₆), -139.82 (PF₆), -135.43 (PF₆); IR (cm⁻¹): ν N–H stretching (3616, 3379), sp C–H stretching (3336), Arm C–H stretching (3145), sp³ C–H stretching (2964), N–H bending (1606), sp³ C–H bending (1458), Arm C=C stretching (1367), C–N stretching (1199), P–F stretching (831), C–H bending (692); LCMS (MeOH): *m/z*: 667.2 [M]⁺.

[(η⁶-*p*-Cymene)RuCl(K²-*N,N*-2-(4-(*p*-tolylethynyl)phenyl)-1*H*-imidazo[4,5-*f*][1,10]phenanthroline)]-PF₆ (**17b**). 52.9 mg (0.0640 mmol, 98%); Mr (C₃₈H₃₂N₄ClF₆PRu) = 826.15 g mol⁻¹; Anal. Calcd for C₃₈H₃₂N₄ClF₆PRu: C 55.24, H 3.90, N 6.78; found: C 55.56; H 3.54; N 7.10; m.p.: 146–148 °C; *R*_f (100% methanol): 0.71; ¹H NMR (DMSO-*d*₆, 400 MHz): δ 0.90 (d, 6H, *J* = 8 Hz, cymene isopropyl-CH₃), 2.2 (s, 3H, cymene CH₃), 2.29 (s, 3H, CH₃), 2.60–2.68 (m, 1H, cymene CH), 6.11 (d, 2H, *J* = 8 Hz, cymene ArH), 6.33 (d, 2H, *J* = 8 Hz, cymene ArH), 7.46 (d, 2H, *J* = 8 Hz, ArH), 7.57–7.65 (m, 4H, ArH), 8.21 (s, 2H, ArH), 8.26 (d, 1H, *J* = 8 Hz, ArH), 8.38 (d, 1H, *J* = 8 Hz, ArH), 9.33 (s, 2H, ArH), 9.86 (s, 2H, ArH); ¹³C NMR (DMSO-*d*₆, 100 MHz): δ 18.3 (Me, *p*-cymene), 21.9 (Me, *p*-cymene), 22.1 (Me, *p*-cymene), 24.4 (Me, ligand), 30.5 (CH, *p*-cymene), 82.3 (ArCH, *p*-cymene), 84.4 (ArCH, *p*-cymene), 85.9 (ArCH, *p*-cymene), 86.8 (ArCH, *p*-cymene), 100.6 (ArC, *p*-cymene), 102.2 (ArC, *p*-cymene), 107.0, 129.5, 126.5, 126.8, 127.0, 129.0, 129.2, 129.2, 129.3, 129.5, 129.7, 131.9, 132.0, 132.9, 143.6, 154.3; ¹⁹F NMR (DMSO-*d*₆, 376 MHz): δ -71.07 (PF₆), -69.18 (PF₆); ³¹P NMR (DMSO-*d*₆, 162 MHz): δ -152.98 (PF₆), -148.60 (PF₆), -144.20 (PF₆), -139.82 (PF₆), -135.43 (PF₆); IR (cm⁻¹): ν N–H stretching (3317), Arm C–H stretching (3161), N–H bending (1606), Arm C=C stretching (1409), C–N stretching (1116), P–F stretching (831), C–H bending (696); LCMS (MeOH): *m/z*: 681.4 [M]⁺.

[(η⁶-*p*-Cymene)RuCl(K²-*N,N*-2-(4-(4-methoxyphenyl)ethynyl)phenyl)-1*H*-imidazo[4,5-*f*][1,10]phenanthroline)]-PF₆ (**17c**). 52.8 mg (0.0627 mmol, 96%); Mr (C₃₈H₃₂N₄OClF₆PRu) = 842.17 g mol⁻¹; Anal. Calcd for C₃₈H₃₂N₄OClF₆PRu: C 54.19, H 3.83, N 6.65; found: C 54.46; H 3.64; N 6.90; m.p.: 138–140 °C; *R*_f (100% methanol): 0.67; ¹H NMR (DMSO-*d*₆, 400 MHz): δ 0.91 (d, 6H, *J* = 8 Hz, cymene isopropyl-CH₃), 2.2 (s, 3H, cymene CH₃), 2.60–2.68 (m, 1H, cymene CH), 3.75 (s, 3H, OCH₃), 6.10 (d, 2H, *J* = 8 Hz, cymene ArH), 6.34 (d, 2H, *J* = 8 Hz, cymene ArH), 7.58 (s, 2H, ArH), 7.60–7.65 (m, 4H, ArH), 8.21 (t, 2H, *J* = 4 Hz, ArH), 8.25 (d, 1H, *J* = 8 Hz, ArH), 8.37 (d, 1H, *J* = 8 Hz, ArH), 9.32 (d, 2H, *J* = 8 Hz, ArH), 9.87 (d, 2H, *J* = 4 Hz, ArH); ¹³C NMR (DMSO-*d*₆, 100 MHz): δ 18.8 (Me, *p*-cymene), 21.9 (Me, *p*-cymene), 22.0 (Me, *p*-cymene), 30.9 (CH, *p*-cymene), 55.5 (OMe, ligand), 84.2 (ArCH, *p*-cymene), 85.9 (ArCH, *p*-cymene), 86.7 (ArCH, *p*-cymene), 86.8 (ArCH, *p*-cymene), 100.7 (ArC, *p*-cymene), 103.9 (ArC, *p*-cymene), 107.1, 114.3, 126.5, 126.8, 127.1, 129.2, 129.3, 129.7, 130.4, 131.8, 131.9, 132.9, 143.6, 154.2; ¹⁹F NMR (DMSO-*d*₆, 376 MHz): δ -71.08 (PF₆), -69.19 (PF₆); ³¹P NMR (DMSO-*d*₆, 162 MHz): δ -152.98 (PF₆), -148.60 (PF₆), -144.20 (PF₆), -139.82 (PF₆), -135.43 (PF₆); IR (cm⁻¹): ν Arm C–H stretching (3147), sp³ C–H stretching (2962), N–H bending (1602), Arm

C=C stretching (1408), C–O stretching (1249), C–N stretching (1174), P–F stretching (831), C–H bending (721); LCMS (MeOH): m/z : 693.3 [M]⁺.

[(η^6 -*p*-Cymene)RuCl(K²-*N,N*-2-(4-(pyridin-2-yl-ethynyl)phenyl)-1*H*-imidazo[4,5-*f*][1,10]phenanthroline)]PF₆ (**17d**). 51.5 mg (0.0634 mmol, 97%); Mr (C₃₆H₂₉N₅ClF₆PRu) = 813.13 g mol⁻¹; Anal. Calcd for C₃₆H₂₉N₅ClF₆PRu: C 53.18, H 3.59, N 8.61; found: C 53.42; H 3.79; N 8.20; m.p.: 134–136 °C; *R*_f (100% methanol): 0.62; ¹H NMR (DMSO-*d*₆, 3 MHz): δ 0.93 (d, 6H, *J* = 8 Hz, cymene isopropyl-CH₃), 2.2 (s, 3H, cymene CH₃), 2.63–2.68 (m, 1H, cymene CH), 6.13 (d, 2H, *J* = 8 Hz, cymene ArH), 6.35 (d, 2H, *J* = 4 Hz, cymene ArH), 7.55–7.58 (m, 2H, ArH), 7.62–7.67 (m, 4H, ArH), 8.22–8.25 (m, 2H, ArH), 8.40 (d, 2H, *J* = 8 Hz, ArH), 9.32 (d, 2H, *J* = 4 Hz, ArH), 9.88 (d, 2H, *J* = 4 Hz, ArH); ¹³C NMR (DMSO-*d*₆, 100 MHz): δ 18.7 (Me, *p*-cymene), 21.9 (Me, *p*-cymene), 22.0 (Me, *p*-cymene), 31.1 (CH, *p*-cymene), 84.3 (ArCH, *p*-cymene), 84.7 (ArCH, *p*-cymene), 85.9 (ArCH, *p*-cymene), 86.8 (ArCH, *p*-cymene), 100.8 (ArC, *p*-cymene), 103.9 (ArC, *p*-cymene), 107.1, 126.5, 126.7, 129.2, 129.3, 129.4, 131.8, 131.9, 132.7, 143.8, 154.2; ¹⁹F NMR (DMSO-*d*₆, 376 MHz): δ -71.07 (PF₆), -69.18 (PF₆); ³¹P NMR (DMSO-*d*₆, 162 MHz): δ -157.38 (PF₆), -152.98 (PF₆), -148.60 (PF₆), -144.20 (PF₆), -139.81 (PF₆), -135.43 (PF₆); IR (cm⁻¹): ν sp² C–H stretching (3053), Arm C–H stretching (2968), N–H bending (1606), sp³ C–H bending (1409), Arm C=C stretching (1325), C–N stretching (1147), C–O stretching (1055), P–F stretching (833), C–H bending (721); LCMS (MeOH): m/z : 668.1 [M]⁺.

Synthesis of [(η^6 -*p*-cymene)RuCl(K²-*N,N*-4-(1*H*-imidazo[4,5-*f*][1,10]phenanthroline-2-yl)phenol)]PF₆ analogues (**19a–c**)

First, 20 mg (0.033 mmol) of dichloro(*p*-cymene)ruthenium(II) dimer (**15**) was dissolved in 7 ml of methanol in a 50 ml round-bottom flask and stirred for 10 min to dissolve the compound in the methanol. Thereafter, 2.1 equivalent of the previously prepared ligand **18a–c** (**18a**: 22.8 mg, **18b**: 22.6 mg, **18c**: 23.7 mg) was added to the reaction mixture followed by magnetic stirring for another 2 h. A change in colour occurred from deep yellow to black. Then, 13 mg (0.082 mmol, 2.5 equiv.) of NH₄PF₆ was added to the reaction mixture and the mixture stirred for another 1 h. The reaction was monitored by TLC using 100% methanol as the solvent system. After completion of the reaction, the methanol was evaporated off using a rotary evaporator and the crude product was further recrystallized from a diethyl ether/methanol mixture. Black fine crystals of complexes **19a–c** were obtained in high yields (~95–97%).

[(η^6 -*p*-Cymene)RuCl(K²-*N,N*-4-(1*H*-imidazo[4,5-*f*][1,10]phenanthroline-2-yl)benzene 1,3 diol)]PF₆ (**19a**). 47.1 mg (0.0634 mmol, 97%); Mr (C₂₉H₂₆N₄O₂ClF₆PRu) = 744.03 g mol⁻¹; Anal. Calcd for C₂₉H₂₆N₄O₂ClF₆PRu: C 46.81, H 3.52, N 7.53; Found: C 46.46; H 3.81; N 7.70; m.p.: 178–180 °C; *R*_f (100% methanol): 0.47; ¹H NMR (DMSO-*d*₆, 400 MHz): δ 0.90 (d, 6H, *J* = 8 Hz, cymene isopropyl-CH₃), 2.19 (s, 3H, cymene CH₃), 2.57–2.66 (m, 1H, cymene CH), 6.10 (d, 2H, *J* = 8 Hz, cymene ArH), 6.33 (d, 2H, *J* = 8 Hz, cymene ArH), 6.48 (s, 1H, ArH), 6.53 (d, 1H, *J* = 8 Hz, ArH), 8.12–8.17 (m, 1H, ArH), 8.19 (d, 2H, *J* = 4 Hz, ArH), 9.35 (d, 2H, *J* = 8 Hz, ArH), 9.84 (d, 2H,

J = 4 Hz, ArH) 9.94 (d, 1H, OH), 9.97 (d, 1H, OH); ¹³C NMR (DMSO-*d*₆, 100 MHz): δ 18.7 (Me, *p*-cymene), 21.8 (Me, *p*-cymene), 21.9 (Me, *p*-cymene), 31.1 (CH, *p*-cymene), 84.2 (ArCH, *p*-cymene), 85.9 (ArCH, *p*-cymene), 86.7 (ArCH, *p*-cymene), 86.8 (ArCH, *p*-cymene), 100.8 (ArC, *p*-cymene), 103.6 (ArC, *p*-cymene), 104.3, 107.2, 126.7, 129.4, 132.9, 143.3, 154.2, 159.4, 161.3; ¹⁹F NMR (DMSO-*d*₆, 376 MHz): δ -71.07 (PF₆), -69.18 (PF₆); ³¹P NMR (DMSO-*d*₆, 162 MHz): δ -157.38 (PF₆), -152.98 (PF₆), -148.60 (PF₆), -144.20 (PF₆), -139.81 (PF₆), -135.43 (PF₆); IR (cm⁻¹): ν sp² C–H stretching (3053), Arm C–H stretching (2968), N–H bending (1606), sp³ C–H bending (1409), Arm C=C stretching (1325), C–N stretching (1147), C–O stretching (1055), P–F stretching (833), C–H bending (721); LCMS (MeOH): m/z : 599.7 [M]⁺.

[(η^6 -*p*-Cymene)RuCl(K²-*N,N*-2-(1*H*-imidazo[4,5-*f*][1,10]phenanthroline-2-yl)-5-methylphenol)]PF₆ (**19b**). 47.0 mg (0.0634 mmol, 97%); Mr (C₃₀H₂₈N₄OClF₆PRu) = 742.06 g mol⁻¹; Anal. Calcd for C₃₀H₂₈N₄OClF₆PRu: C 48.56, H 3.80, N 7.55; found: C 48.26; H 3.44; N 7.70; m.p.: 142–144 °C; *R*_f (100% methanol): 0.61; ¹H NMR (DMSO-*d*₆, 400 MHz): δ 0.86 (d, 6H, *J* = 8 Hz, cymene isopropyl-CH₃), 2.18 (s, 3H, cymene CH₃), 2.32 (s, 3H, CH₃), 2.55–2.61 (m, 1H, cymene CH), 6.07 (d, 2H, *J* = 8 Hz, cymene ArH), 6.30 (d, 2H, *J* = 8 Hz, cymene ArH), 8.12 (t, 3H, *J* = 4 Hz, ArH), 8.20 (d, 1H, *J* = 8 Hz, ArH), 8.27 (d, 1H, *J* = 8 Hz, ArH), 9.27 (d, 2H, *J* = 8 Hz, ArH), 9.77 (d, 1H, *J* = 4 Hz, ArH) 9.95 (d, 1H, *J* = 8 Hz, ArH); ¹³C NMR (DMSO-*d*₆, 100 MHz): δ 18.3 (Me, *p*-cymene), 21.9 (Me, *p*-cymene), 22.1 (Me, *p*-cymene), 24.2 (Me, ligand), 31.1 (CH, *p*-cymene), 84.3 (ArCH, *p*-cymene), 85.9 (ArCH, *p*-cymene), 86.7 (ArCH, *p*-cymene), 86.8 (ArCH, *p*-cymene), 100.7 (ArC, *p*-cymene), 104.4 (ArC, *p*-cymene), 107.0, 118.0, 119.7, 121.0, 133.0, 140.5, 143.5, 154.4, 157.5, 162.0; ¹⁹F NMR (DMSO-*d*₆, 376 MHz): δ -71.07 (PF₆), -69.18 (PF₆); ³¹P NMR (DMSO-*d*₆, 162 MHz): δ -157.38 (PF₆), -152.99 (PF₆), -148.60 (PF₆), -144.21 (PF₆), -139.82 (PF₆), -135.43 (PF₆); IR (cm⁻¹): ν Arm C–H stretching (3140), sp³ C–H stretching (3047), N–H bending (1606), sp³ C–H bending (1409), Arm C=C stretching (1352), C–N stretching (1201), C–O stretching (1147), P–F stretching (831), C–H bending (721); LCMS (MeOH): m/z : 597.7 [M]⁺.

[(η^6 -*p*-Cymene)RuCl(K²-*N,N*-2-(1*H*-imidazo[4,5-*f*][1,10]phenanthroline-2-yl)-5-methoxyphenol)]PF₆ (**19c**). 48.1 mg (0.0634 mmol, 97%); Mr (C₃₀H₂₉N₄O₂ClF₆PRu) = 759.06 g mol⁻¹; Anal. Calcd for C₃₀H₂₉N₄O₂ClF₆PRu: C 47.47, H 3.85, N 7.38; found: C 47.86; H 3.64; N 7.60; m.p.: 138–140 °C; *R*_f (100% methanol): 0.53; ¹H NMR (DMSO-*d*₆, 400 MHz): δ 0.89 (d, 6H, *J* = 8 Hz, cymene isopropyl-CH₃), 2.18 (s, 3H, cymene CH₃), 2.58–2.67 (m, 1H, cymene CH), 3.84 (s, 3H, OCH₃), 6.11 (d, 2H, *J* = 8 Hz, cymene ArH), 6.34 (d, 2H, *J* = 8 Hz, cymene ArH), 8.18 (m, 3H, ArH), 8.27 (d, 2H, *J* = 8 Hz, ArH), 9.37 (d, 2H, *J* = 8 Hz, ArH), 9.84 (d, 2H, *J* = 8 Hz, ArH) 9.96 (m, 1H, OH); ¹³C NMR (DMSO-*d*₆, 100 MHz): δ 18.7 (Me, *p*-cymene), 21.9 (Me, *p*-cymene), 22.0 (Me, *p*-cymene), 31.1 (CH, *p*-cymene), 55.9 (OMe, ligand), 84.3 (ArCH, *p*-cymene), 85.9 (ArCH, *p*-cymene), 86.7 (ArCH, *p*-cymene), 86.8 (ArCH, *p*-cymene), 102.0 (ArC, *p*-cymene), 103.6 (ArC, *p*-cymene),

104.3, 107.3, 126.6, 128.5, 132.9, 143.4, 154.2, 159.4, 162.8; ^{19}F NMR (DMSO- d_6 , 376 MHz): δ -71.08 (PF₆), -69.19 (PF₆); ^{31}P NMR (DMSO- d_6 , 162 MHz): δ -152.98 (PF₆), -148.59 (PF₆), -144.20 (PF₆), -139.81 (PF₆), -135.43 (PF₆), -131.03 (PF₆); IR (cm⁻¹): ν Arm C-H stretching (3053), sp³ C-H stretching (2935), N-H bending (1627), Arm C=C stretching (1446), C-N stretching (1261), C-O stretching (1151), P-F stretching (833), C-H bending (721); LCMS (MeOH): m/z : 613.4 [M]⁺.

In vitro cytotoxic study

In vitro cytotoxicity was evaluated using the standard MTT assay protocol.⁶³ The synthesized complexes (**16a-b**, **17a-d** and **19a-c**) were dissolved in 0.1% DMSO and then serially diluted with DMEM medium. Two cancer cell lines, *i.e.* human epithelioid cervix carcinoma (HeLa), human epithelial colorectal adenocarcinoma cells (Caco-2), and one normal kidney cell (HEK 293), were used in this assay. Approximately 1×10^4 cells per well were cultured in 100 μl of a growth medium in 96-well plates and incubated at 37 °C under a 5% CO₂ atmosphere. The cells were then treated with different concentrations of the drugs (0–200 μM) in a volume of 100 μM per well. Cisplatin and RAPTA-C were used as standard positive control drugs. Cells in the control wells also acquired the same volume of medium containing 0.1% DMSO. After 24 h, the medium was superfluous and the cell cultures were incubated with 100 μl MTT reagent (1 mg ml⁻¹) for 5 h at 37 °C. Then, the suspension was placed on a micro vibrator for 10 min followed by recording the absorbance at $\lambda = 620$ nm in an ELISA reader. The experiment was also performed in triplicate. The data were represented as the growth inhibition percentage, *i.e.* % growth inhibition = $100 - [(AD \times 100)/AB]$, where AD is the measured absorbance in the wells containing the samples and AB is the measured absorbance for the blank wells (cells with a medium and a vehicle only).

Stability study

The stabilities of the three Ru(II) complexes (**16b**, **17a** and **19b**) were tested in 1% DMSO in PBS buffer as the complexes were dissolved in this solution during their cytotoxicity and imaging studies.

DNA binding study

The binding of the complexes with calf-thymus DNA (CT-DNA) was observed by their electronic spectra and through a competitive binding assay using ethidium bromide (EtBr) as a quencher in fluorescence spectroscopy.

UV-visible studies

A DNA binding assay was carried out by using complexes **4**, **4'**, **5** and **5'** in Tris-HCl buffer (5 mM Tris-HCl in water, pH 7.4) in a water medium.⁶⁴ The concentration of CT-DNA was calculated from its absorbance intensity at 260 nm and its known molar absorption coefficient value 6600 M⁻¹ cm⁻¹. An equal amount of DNA was taken both in the sample and in the reference in cuvettes. Titration was carried out by increasing the concentration of CT-DNA. Before each measurement, each

sample was equilibrated with CT-DNA for about 5 min then absorbance of the complex was measured. The intrinsic DNA binding constant (K_b) was calculated using the eqn (i):

$$\frac{[\text{DNA}]}{(\varepsilon_a - \varepsilon_f)} = \frac{[\text{DNA}]}{(\varepsilon_b - \varepsilon_f)} + \frac{1}{K_b(\varepsilon_a - \varepsilon_f)} \quad (\text{i})$$

where [DNA] is the concentration of DNA in the base pairs, ε_a is the apparent extinction coefficient observed for the complex, ε_f corresponds to the extinction coefficient of the complex in its free form and ε_b refers to the extinction coefficient of the complex when fully bound to DNA. Data were plotted using Origin Lab, version 8.5 to obtain the [DNA]/($\varepsilon_a - \varepsilon_f$) vs. [DNA] linear plot. The ratio of the slope to the intercept from the linear fit gives the value of the intrinsic binding constant (K_b).

UV and fluorescence study

UV and fluorescence studies of all these Ru(II) complexes, were performed in 5% DMSO-buffer solution. The fluorescence quantum yields (Φ) were calculated by using the comparative William's method, which involves the use of a well-characterized standard with a known quantum yield value using 5% DMSO in PBS buffer solution.⁶⁵ Quinine sulphate was used as the standard. The quantum yield was calculated according to the eqn (ii):

$$\phi = \phi_R \times \frac{I_S}{I_R} \times \frac{\text{OD}_R}{\text{OD}_S} \times \frac{\eta_S}{\eta_R} \quad (\text{ii})$$

where ϕ is the quantum yield, I is the peak area, OD is the absorbance at λ_{max} and η is the refractive index of the solvent (S) and reference (R). Here, we used quinine sulphate as the standard for calculating the quantum yield.

Ethidium bromide displacement assay

The ethidium bromide (EtBr) displacement assay was carried out to explain the mode of binding between the potent compounds with DNA.⁶⁶ The apparent binding constants (K_{app}) of the complexes **16b**, **17a** and **19b** to CT-DNA were calculated using ethidium bromide (EtBr) as a spectral probe in 5 mM Tris-HCl buffer (pH 7.4). Here, EtBr does not exhibit any fluorescence in its free form as its fluorescence is quenched by the solvent molecules, but its fluorescence intensity increases in the presence of CT-DNA, which suggests the intercalative mode of binding of EtBr with DNA grooves. The fluorescence intensity was found to decrease with a further increase in concentration of the complexes. Thus, it can be said that the complexes displace EtBr from the CT-DNA grooves and the complexes themselves then get bound to the DNA base pairs. The values of the apparent binding constant (K_{app}) were obtained by using eqn (iii):

$$K_{\text{app}} \times [\text{Complex}]_{50} = K_{\text{EtBr}} \times [\text{EtBr}] \quad (\text{iii})$$

where K_{EtBr} is the EtBr binding constant ($K_{\text{EtBr}} = 1.0 \times 10^7$ M⁻¹), and [EtBr] = 8×10^{-6} M. The Stern-Volmer equation has been employed for the quantitative determination of the Stern-Volmer quenching constant (K_{SV}).⁶⁷ Origin Lab (8.5)

software was used to plot the fluorescence data to obtain a linear plot of I_0/I vs. [complex]. The value of K_{SV} was calculated from the following equation.

$$I_0/I = 1 + K_{SV}[Q] \quad (\text{iv})$$

where I_0 is the fluorescence intensity in the absence of a complex and I is the fluorescence intensity in the presence of a complex of concentration $[Q]$.

Protein-binding studies

Serum albumin proteins are major components in blood plasma proteins and play significant roles in drug transport and metabolism.⁶⁸ The interaction of the drug with bovine serum albumin (BSA), a structural homologue with human serum albumin (HSA), has been studied in tryptophan emission quenching experiments. Tryptophan emission quenching experiment was thus performed here to detect the interaction of the ruthenium complexes **16b**, **17a** and **19b** with protein BSA. Initially, BSA solution (2×10^{-6} M) was prepared in Tris-HCl/NaCl buffer. Aqueous solutions of the complexes were subsequently added to the BSA solution with increasing their concentrations. After each addition, the solutions were shaken slowly for 5 min before recording the fluorescence at a wavelength of 295 nm ($\lambda_{\text{ex}} = 295$ nm). A gradual decrease in fluorescence intensity of BSA at $\lambda = 340$ nm was observed upon increasing the concentration of the complex, which confirmed that an interaction between the complex and BSA had occurred. The Stern–Volmer equation was employed to quantitatively determine the quenching constant (K_{BSA}). Origin Lab, version 8.5 was used to plot the emission spectral data to obtain a linear plot of I_0/I vs. [complex] using the following eqn (v):

$$I_0/I = 1 + K_{\text{BSA}}[Q] = 1 + k_q\tau_0[Q] \quad (\text{v})$$

where I_0 is the fluorescence intensity of BSA in the absence of the complex and I indicates the fluorescence intensity of BSA in the presence of the complex of concentration $[Q]$, τ_0 is the lifetime of the tryptophan in BSA and was found to be 1×10^{-8} and k_q is the quenching constant. The Scatchard eqn (vi) was used to give the binding properties of the complexes,⁶⁹ where K is the binding constant and n is the number of binding sites.

$$\log(I_0 - I/I) = \log K + n \log[Q] \quad (\text{vi})$$

Conductivity measurement

To confirm the interaction of the complexes with water, DMSO, GSH and CT-DNA solutions, conductivity tests of the prepared complexes were performed using a conductivity-TDS meter-307 (Systronics, India) and a cell constant of 1.0 cm^{-1} .⁷⁰ The rate of conductivity was also measured in different pH media. Time-dependent conductivity measurements were also performed.

n-Octanol–water partition coefficient (log *P*)

The log *P* values of the ruthenium complexes were determined via the shake flask method using the previously published procedure.⁷¹ A known amount of each complex (**16a–b**, **17a–d** and **19a–b**) was suspended in water (pre-saturated with *n*-octanol) and shaken for 48 h on an orbital shaker. To allow the phase separation, the solution was centrifuged for 10 min at 3000 rpm. Then, the amount of ruthenium present in the saturated aqueous solution was measured by ICP-MS. To obtain the partition coefficient, different ratios (0.5 : 1, 1 : 1 and 2 : 1) of the saturated solutions were shaken with pre-saturated *n*-octanol for 20 min on an orbital shaker and followed the same procedure.

Conclusion

In summary, we synthesized and characterized some novel imidazophenanthroline ligands and their ruthenium(II)-*p*-cymene complexes. The ligands were prepared by following a novel procedure of microwave-assisted Suzuki and Sonogashira cross-coupling reactions. The stability study of the three complexes **16b**, **17a** and **19b** in DMSO-buffer solution indicated that all three complexes were fairly stable in DMSO-buffer solution conditions from 0 to 48 h. From the DNA binding studies, it was observed that the intrinsic binding constant (K_b) values were in the order of **19b** > **16b** > **17a**, whereas the apparent binding constant (K_{app}) was observed in the order of **16b** > **17a** > **19b**, which could be correlated to the fact that complex **16b** intercalates DNA double strands more effectively than other derivatives because of its planarity. The significant hyperchromism in the absorbance spectra of the DNA binding curve, high conductance in aqueous DMSO, high K_{app} value along with the results from the viscosity study indicated a covalent and non-covalent mode of binding of the complexes with DNA. The BSA binding study also revealed that complex **19b** had a many folds greater binding efficiency with BSA compared to **16b** and **17a**. However, the number of binding sites of BSA was more for **16b**. The cytotoxicity study indicated that complex, **16b** displayed the best potency and selectivity with both cancer cells. Live-cell imaging with the moderately fluorescent compound **17a** in HeLa cell suggested that it was intensely consumed by the HeLa cell after 2 h.

Conflicts of interest

There are no conflicts to declare.

Acknowledgements

Authors are grateful to Department of Science and Technology, Government of India for supporting the work through the DST-EMR project grant (EMR/2017/000816) and DST young scientist grant (YSS/2014/000842). The authors are thankful to

VIT University for providing VIT SEED funding. Authors are also thankful to DST-VITFIST for NMR and GC-MS for research facilities.

Notes and references

- M. Heron, Deaths: leading causes for 2010, *Natl. Vital Stat. Rep.*, 2013, **62**, 1–97.
- C. Zhang and S. Lippard, *Curr. Opin. Chem. Biol.*, 2003, **7**, 481–489.
- K. Hariprasath, B. Deepthi, I. Sudheer Babu, P. Venkatesh, S. Sharfudeen and V. Soumya, *J. Chem. Pharm. Res.*, 2010, **2**, 496–499.
- I. Warad, A. Eftaiha, M. Nuri, I. Ahmad, A. Husein and M. Assal, *J. Mater. Environ. Sci.*, 2013, **4**, 542–557.
- R. Raj Kumar, R. Ramesh and J. G. Małecki, *J. Organomet. Chem.*, 2018, **862**, 95–100.
- C. Hartinger and P. J. Dyson, *Chem. Soc. Rev.*, 2009, **38**, 391–401.
- A. M. Pizarro, A. Habtemariam and P. J. Sadler, in *Medicinal Organometallic Chemistry*, Springer-Verlag, 2010, vol. 32, pp. 21–56.
- A. Casini, C. G. Hartinger, A. A. Nazarov and P. J. Dyson, in *Medicinal Inorganic Chemistry*, Springer-Verlag, 2010, vol. 32, pp. 57–80.
- I. Bratsos, T. Gianferrara, E. Alessio, C. G. Hartinger, M. A. Jakupec and B. K. Keppler, *Bioinorganic Medicinal Chemistry*, Wiley-VCH, 2011, pp. 151–174.
- E. R. Jamieson and S. J. Lippard, *Chem. Rev.*, 1999, **99**, 2467–2498.
- G. Chu, *J. Biol. Chem.*, 1994, **269**, 787–790.
- V. Cepeda, M. A. Fuertes, J. Castilla, C. Alonso, C. Quevedo and J. M. Pérez, *Anti-Cancer Agents Med. Chem.*, 2007, **7**, 3–18.
- S. Dhar, F. X. Gu, R. Langer, O. C. Farokhzad and S. J. Lippard, *Proc. Natl. Acad. Sci. U. S. A.*, 2008, **105**, 17356–17361.
- S. Dhar, Z. Liu, J. Thomale, H. Dai and S. J. Lippard, *J. Am. Chem. Soc.*, 2008, **130**, 11467–11476.
- X.-J. Liang, H. Meng, Y. Wang, H. He, J. Meng, J. Lu, P. C. Wang, Y. Zhao, X. Gao and B. Sun, *Proc. Natl. Acad. Sci. U. S. A.*, 2010, **107**, 7449–7454.
- T. T.-H. Fong, C.-N. Lok, C. Y.-S. Chung, Y.-M. E. Fung, P.-K. Chow, P.-K. Wan and C.-M. Che, *Angew. Chem., Int. Ed.*, 2016, **55**, 11935–11939.
- Z.-T. Cao, Z.-Y. Chen, C.-Y. Sun, H.-J. Li, H.-X. Wang, Q.-Q. Cheng, Z.-Q. Zuo, J.-L. Wang, Y.-Z. Liu, Y.-C. Wang and J. Wang, *Biomaterials*, 2016, **94**, 9–19.
- H. Huang, P. Zhang, Y. Chen, K. Qiu, C. Jin, L. Ji and H. Chao, *Dalton Trans.*, 2016, **45**, 13135.
- I. Arany and R. L. Safirstein, *Semin. Nephrol.*, 2003, **23**, 460–464.
- A.-M. Florea and D. Büsselberg, *Cancers*, 2011, **3**, 1351–1371.
- L. Galluzzi, L. Senovilla, I. Vitale, J. Michels, I. Martins, O. Kepp, M. Castedo and G. Kroemer, *Oncogene*, 2012, **31**, 1869–1883.
- Y.-R. Zheng, K. Suntharalingam, T. C. Johnstone, H. Yoo, W. Lin, J. G. Brooks and S. J. Lippard, *J. Am. Chem. Soc.*, 2014, **136**, 8790–8798.
- K. Suntharalingam, Y. Song and S. J. Lippard, *Chem. Commun.*, 2014, **50**, 2465–2468.
- N. Graf, D. R. Bielenberg, N. Kolishetti, C. Muus, J. Banyard, O. C. Farokhzad and S. J. Lippard, *ACS Nano*, 2012, **6**, 4530–4539.
- C. S. Allardyce and P. J. Dyson, *Platinum Metals Rev.*, 2001, **45**, 62–69.
- C. G. Hartinger, M. Groessl, S. M. Meier, A. Casini and P. J. Dyson, *Chem. Soc. Rev.*, 2013, **42**, 6186–6199.
- E. S. Antonarakis and A. Emadi, *Cancer Chemother. Pharmacol.*, 2010, **66**, 1–9.
- A. I. Minchinton and I. F. Tannock, *Nat. Rev. Cancer*, 2006, **6**, 583–592.
- S. Thota, D. A. Rodrigues, D. C. Crans and E. J. Barreiro, *J. Med. Chem.*, 2018, **61**, 5805–5821.
- J. Chen, L. Chen, S. Liao, K. Zheng and L. Ji, *J. Phys. Chem. B*, 2007, **111**, 7862–7869.
- M. Bacac, A. C. Hotze, K. van der Schilden, J. G. Haasnoot, S. Pacor, E. Alessio, G. Sava and J. Reedijk, *J. Inorg. Biochem.*, 2004, **98**, 402–412.
- J. M. Rademaker-Lakhai, D. van den Bongard, D. Pluim, J. H. Beijnen and J. H. Schellens, *Clin. Cancer Res.*, 2004, **10**, 3717–3727.
- C. G. Hartinger, S. Zorbas-Seifried, M. A. Jakupec, B. Kynast, H. Zorbas and B. K. Keppler, *J. Inorg. Biochem.*, 2006, **100**, 891–904.
- C. G. Hartinger, M. A. Jakupec, S. Zorbas-Seifried, M. Groessl, A. Egger, W. Berger, H. Zorbas, P. J. Dyson and B. K. Keppler, *Chem. Biodiversity*, 2008, **5**, 2140–2155.
- A. K. Bytzek, G. Koellensperger, B. K. Keppler and C. G. Hartinger, *J. Inorg. Biochem.*, 2016, **160**, 250–255.
- P. J. Dyson, *Chimia*, 2017, **61**, 698–670.
- A. Habtemariam, M. Melchart, R. Fernández, S. Parsons, I. D. H. Oswald, A. Parkin, F. P. A. Fabbiani, J. E. Davidson, A. Dawson, R. E. Aird, D. I. Jodrell and P. J. Sadler, *J. Med. Chem.*, 2006, **49**, 6858–6868.
- N. P. Barry and P. J. Sadler, *Chem. Commun.*, 2013, **49**, 5106–5131.
- S. B. Lara, L. Salassa, A. Habtemariam, O. Novakova, A. M. Pizarro, G. J. Clarkson, B. Liskova, V. Brabec and P. J. Sadler, *Organometallics*, 2012, **31**, 3466–3479.
- A. C. Komor and J. K. Barton, *Chem. Commun.*, 2013, **49**, 3617–3630.
- A. Casini, G. Mastrobuoni, W. H. Ang, C. Gabbiani, G. Pieraccini, G. Moneti, P. J. Dyson and L. Messori, *ChemMedChem*, 2007, **2**, 631–635.
- R. Zhao, R. Hammitt, R. P. Thummel, Y. Liu, C. Turro and R. M. Snapka, *Dalton Trans.*, 2009, 10926–10931.
- L. Zeng, Y. Xiao, J. Liu and L. Tan, *J. Mol. Struct.*, 2012, **1019**, 183–190.

- 44 R. E. Aird, J. Cummings, A. A. Ritchie, M. Muir, R. E. Morris, H. Chen, P. J. Sadler and D. I. Jodrell, *Br. J. Cancer*, 2002, **86**, 1652–1657.
- 45 G. I. Pascu, A. C. Hotze, C. Sanchez-Cano, B. M. Kariuki and M. J. Hannon, *Angew. Chem.*, 2007, **119**, 4452–4456.
- 46 K. Wu, W. Hu, Q. Luo, X. Li, S. Xiong, P. J. Sadler and F. Wang, *J. Am. Soc. Mass Spectrom.*, 2013, **24**, 410–420.
- 47 R. E. Morris, R. E. Aird, P. del S. Murdoch, H. Chen, J. Cummings, N. D. Hughes, S. Parsons, A. Parkin, G. Boyd, D. I. Jodrell and P. J. Sadler, *J. Med. Chem.*, 2001, **44**, 3616–3621.
- 48 H. Chen, J. A. Parkinson, S. Parsons, R. A. Coxall, R. O. Gould and P. J. Sadler, *J. Am. Chem. Soc.*, 2002, **124**, 3064–3082.
- 49 H. Chen, J. A. Parkinson, R. E. Morris and P. J. Sadler, *J. Am. Chem. Soc.*, 2003, **125**, 173–186.
- 50 H. Huang, P. Zhang, B. Yu, Y. Chen, J. Wang, L. Ji and H. Chao, *J. Med. Chem.*, 2014, **57**, 8971–8983.
- 51 (a) A. Notaro and G. Gasser, *Chem. Soc. Rev.*, 2017, **46**, 7317–7337; (b) Y.-J. Liu, H. Chao, Y.-X. Yuan, H.-J. Yu and L.-N. Ji, *Inorg. Chim. Acta*, 2006, **359**, 3807–3814.
- 52 (a) L. Zeng, P. Gupta, Y. Chen, E. Wang, L. Ji, H. Chao and Z. Chen, *Chem. Soc. Rev.*, 2017, **46**, 5771; (b) L.-F. Tan, F. Wang, H. Chao, Y.-F. Zhou and C. Weng, *J. Inorg. Biochem.*, 2007, **101**, 700–708.
- 53 (a) K. A. Kumar, K. L. Reddy and S. Satyanaraya, *Transition Met. Chem.*, 2010, **35**, 713–720; (b) P. J. Jarman, F. Noakes, S. Fairbanks, K. Smitten, I. K. Griffiths, H. K. Saeed, J. A. Thomas and C. Smythe, *J. Am. Chem. Soc.*, 2019, **141**, 2925–2937; (c) B. Pena, S. Saha, R. Barhoumi, R. C. Burghardt and K. R. Dunbar, *Inorg. Chem.*, 2018, **57**, 12777–12786.
- 54 (a) G. R. Jadhav, S. Sinha, M. Chhabra and P. Paira, *Bioorg. Med. Chem. Lett.*, 2016, **26**, 2695–2700; (b) S. K. Subran, S. Banerjee, A. Mondal and P. Paira, *New J. Chem.*, 2016, **40**, 10333–10343; (c) A. Mondal, S. De, S. Maiti, B. Sarkar, A. K. Sk, R. Jacob, A. Moorthy and P. Paira, *J. Photochem. Photobiol., B*, 2018, **178**, 380–394; (d) S. De, S. Ray Chaudhuri, A. Panda, G. R. Jadhav, R. S. Kumar, P. Manohar, N. Ramesh, A. Mondal, A. Moorthy, S. Banerjee, P. Paira and S. K. Ashok Kumar, *New J. Chem.*, 2019, **43**, 3291–3302.
- 55 S. J. Dougan, A. Habtemariam, S. E. McHale, S. Parsons and P. J. Sadler, *Proc. Natl. Acad. Sci. U. S. A.*, 2008, **105**, 11628–11633.
- 56 F. Wang, H. Chen, S. Parsons, I. D. H. Oswald, J. E. Davidson and P. J. Sadler, *Chem. – Eur. J.*, 2003, **9**, 5810–5820.
- 57 T. Bugarcic, A. Habtemariam, R. J. Deeth, F. P. A. Fabbiani, S. Parsons and P. J. Sadler, *Inorg. Chem.*, 2009, **48**, 9444–9453.
- 58 M. Kubanik, H. Holtkamp, T. Söhnel, S. M. F. Jamieson and C. G. Hartinger, *Organometallics*, 2015, **34**, 5658–5668.
- 59 (a) W. J. Geary, *Coord. Chem. Rev.*, 1971, **7**, 81–122; (b) I. Ali, W. A. Wani and K. Saleem, *Synthesis and Reactivity in Inorganic, Metal–Organic, and Nano-Metal Chemistry*, 2013, vol. 43, pp. 1162–1170.
- 60 P. Liu, B. Wu, J. Liu, Y. Dai, Y. Wang and K. Wang, *Inorg. Chem.*, 2016, **55**, 1412–1422.
- 61 B. M. Zeglis, V. C. Pierre and J. K. Barton, *Chem. Commun.*, 2007, **44**, 4565–4579.
- 62 A. N. Boynton, L. Marcélis, A. J. McConnell and J. K. Barton, *Inorg. Chem.*, 2017, **56**, 8381–8389.
- 63 P. Liu, B. Wu, J. Liu, Y. Dai, Y. Wang and K. Wang, *Inorg. Chem.*, 2016, **55**, 1412–1422.
- 64 M. Sirajuddin, S. Ali and A. Badshah, *J. Photochem. Photobiol., B*, 2013, **124**, 1–19.
- 65 M. Shamsi-Sani, F. Shirini, M. Abedini and M. Seddighi, *Res. Chem. Intermed.*, 2016, **42**, 1091–1099.
- 66 S. Dasari and A. K. Patra, *Dalton Trans.*, 2015, **44**, 19844–19855.
- 67 J. Keizer, *J. Am. Chem. Soc.*, 1983, **105**, 1494–1498.
- 68 V. D. Suryawanshi, L. S. Walekar, A. H. Gore, P. V. Anbhule and G. B. Kolekar, *J. Pharm. Anal.*, 2016, **6**, 56–63.
- 69 K. Jeyalakshmi, J. Haribabu, C. Balachandran, S. Swaminathan, N. S. P. Bhuvanesh and R. Karvembu, *Organometallics*, 2019, **38**, 753–770.
- 70 S. Nikolić, L. Rangasamy, N. Gligorijević, S. Arandelović, S. Radulović, G. Gasser and S. Grgurić-Šipka, *J. Inorg. Biochem.*, 2016, **160**, 156–165.
- 71 M. Kubanik, H. Holtkamp, T. Söhnel, S. M. F. Jamieson and C. G. Hartinger, *Organometallics*, 2015, **34**, 5658–5668.